

Coarse-Grained Boltzmann Generators

Weilong Chen ^{*1} Bojun Zhao ^{*1} Jan Eckwert ¹ Julija Zavadlav ^{1,2}

Abstract

Sampling equilibrium molecular configurations from the Boltzmann distribution is a long-standing challenge. Boltzmann Generators (BGs) address this by combining exact-likelihood generative models with importance sampling, but their practical scalability is limited. Meanwhile, coarse-grained surrogates enable the modeling of larger systems by reducing effective dimensionality, yet often lack the reweighting process required to ensure asymptotically correct statistics. In this work, we propose Coarse-Grained Boltzmann Generators (CG-BGs), a principled framework that unifies scalable reduced-order modeling with the exactness of importance sampling. CG-BGs act in a coarse-grained coordinate space, using a learned potential of mean force (PMF) to reweight samples generated by a flow-based model. Crucially, we show that this PMF can be efficiently learned from rapidly converged data via force matching. Our results demonstrate that CG-BGs faithfully capture complex interactions mediated by explicit solvent within highly reduced representations, establishing a scalable pathway for the unbiased sampling of larger molecular systems.

1. Introduction

Accurately sampling molecular configurations from the Boltzmann distribution is a fundamental challenge in statistical physics (Chandler, 1987). Access to these samples is essential for computing thermodynamic observables, including free energies (Chipot & Pohorille, 2007). For molecular systems, the high dimensionality renders direct evaluation of the partition function intractable, forcing a reliance on simulation methods such as Molecular Dynam-

ics (MD) or Markov Chain Monte Carlo (MCMC) (Frenkel & Smit, 2002). However, these approaches often struggle with the rugged, multi-modal structure of potential energy landscapes. High free-energy barriers trap trajectories in metastable states, leading to highly correlated samples and slow convergence (Lindorff-Larsen et al., 2011). Despite extensive progress in enhanced sampling methods (Zhu et al., 2025; Hénin et al., 2022) (e.g., umbrella sampling (Torrie & Valleau, 1977), metadynamics (Laio & Gervasio, 2008)) and coarse-graining (Noid, 2013; Saunders & Voth, 2013), efficient equilibrium sampling remains a major bottleneck.

Deep generative models have recently emerged as a promising alternative for equilibrium sampling (Noé et al., 2019; Albergo et al., 2019; Wirnsberger et al., 2020). A notable example is the Boltzmann Generator (BG) (Noé et al., 2019). By learning a diffeomorphic transformation between a simple prior (e.g., a Gaussian) and the complex molecular configuration space, BGs enable efficient proposal generation and exact likelihood evaluation. The tractable likelihood permits rigorous reweighting of generated configurations to the target Boltzmann distribution via importance sampling, yielding asymptotically exact equilibrium statistics. This enables amortized sampling (Tan et al., 2025b), where generation cost is substantially lower than MD simulations.

In practice, however, scaling BGs to high-dimensional molecular systems remains challenging (Klein & Noé, 2024; Tan et al., 2025a). As system size increases, even expressive generative models exhibit diminishing overlap with the target distribution, resulting in high-variance importance weights and ineffective reweighting. Moreover, exact likelihood evaluation requires computing Jacobian determinants (Chen et al., 2018), which incurs significant computational overhead and scales poorly with dimensionality (Hutchinson, 1989). As a result, current BGs have mostly been applied to small systems, such as short peptides (Tan et al., 2025b; Rehman et al., 2025), often restricted to empirical implicit solvent models (Hawkins et al., 1995; Nguyen et al., 2013).

Coarse-graining (CG) provides a complementary approach by projecting atomistic configurations onto a lower-dimensional set of collective variables. This idea underlies Boltzmann Emulators (Lewis et al., 2025; Zheng et al., 2024; Jing et al., 2024; Zhu et al., 2026) and related generative surrogates (Daigavane et al., 2025; Schreiner et al., 2023;

^{*}Equal contribution, random order. ¹Professorship of Multi-scale Modeling of Fluid Materials, Department of Engineering Physics and Computation, TUM School of Engineering and Design, Technical University of Munich, Germany ²Atomistic Modeling Center, Munich Data Science Institute, Technical University of Munich, Germany. Correspondence to: Julija Zavadlav <julija.zavadlav@tum.de>.

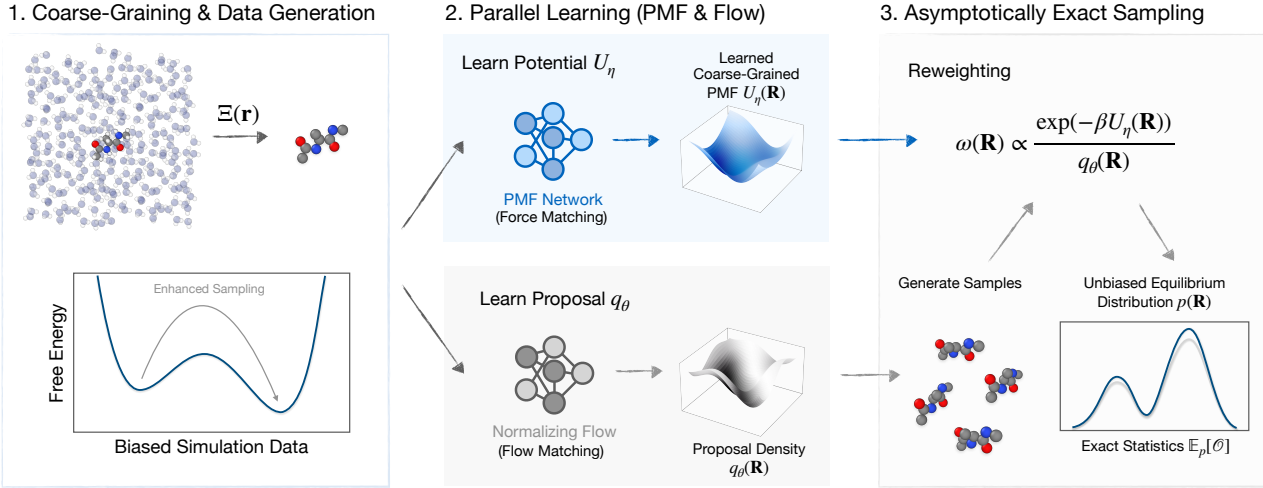


Figure 1. CG-BG workflow. (1) Training data are collected and mapped from atomistic configurations to CG beads. (2) A PMF network learns $U_\eta(\mathbf{R})$ from rapidly converged data, while a normalizing flow learns a proposal density $q_\theta(\mathbf{R})$. (3) CG samples from flow models are reweighted with the PMF to recover the target distribution $p(\mathbf{R})$ and compute unbiased thermodynamic observables.

Plainer et al., 2025; Costa et al., 2025; dos Santos Costa et al., 2024; Diez et al., 2025; Vlachas et al., 2021; Xu et al., 2025), which reduce the number of degrees of freedom and allow models to effectively handle larger systems. However, these approaches face a circular dependency: training generally requires unbiased equilibrium data, which is precisely the computational bottleneck they aim to overcome. In most cases, CG surrogates are often trained on finite-time, non-equilibrium trajectories (Lewis et al., 2025; Zheng et al., 2024) and, unlike Boltzmann Generators, most lack a reweighting procedure to correct for this mismatch, resulting in biased statistics.

Present work. In this paper, we introduce *Coarse-Grained Boltzmann Generators* (CG-BGs, Fig. 1), a class of Boltzmann Generators that operate directly in CG coordinate ¹. CG-BGs combine generative modeling with importance sampling using a learned potential of mean force (PMF) as the target energy, enabling exact equilibrium sampling in a reduced-dimensional representation. This design provides a scalable pathway for sampling high-dimensional molecular systems. CG-BGs are particularly advantageous as they can be trained directly from rapidly converged data and effectively capture complex solvent-mediated effects.

Our main contributions are:

- We introduce **Coarse-Grained Boltzmann Generators**, a scalable framework for equilibrium sampling in CG coordinate space. To our knowledge, this is the first BG formulation that incorporates **machine learning potentials** (MLPs) as the target energy for importance sampling.

¹Our code is publicly available at <https://github.com/tummmfm/cg-bg>.

- We leverage enhanced sampling force matching to learn CG PMFs directly from rapidly converged simulations, eliminating reliance on unbiased equilibrium data and providing a correction mechanism for CG Boltzmann Emulators.
- We demonstrate that CG-BGs capture solvent-mediated interactions in highly reduced representations, achieving improved accuracy over classical implicit solvent models while dramatically reducing computational cost relative to atomistic BGs.

2. Background and Preliminaries

Notation. We use lowercase variables for fine-grained (atomistic) quantities and uppercase variables for CG quantities.

We consider a many-body system with configuration $\mathbf{r} \in \mathbb{R}^n$ governed by a potential energy function $u(\mathbf{r})$. At thermodynamic equilibrium with temperature T , the system follows the Boltzmann distribution

$$p(\mathbf{r}) = \frac{e^{-\beta u(\mathbf{r})}}{Z}, \quad Z = \int e^{-\beta u(\mathbf{r})} d\mathbf{r}, \quad (1)$$

where $\beta = (k_B T)^{-1}$ and Z is the partition function. The goal of equilibrium sampling is to generate samples from $p(\mathbf{r})$ in order to compute observables $\mathbb{E}_p[\mathcal{O}] = \int \mathcal{O}(\mathbf{r}) p(\mathbf{r}) d\mathbf{r}$, and free energies. A dataset is considered converged if the empirical averages of observables statistically recover equilibrium expectations.

2.1. Boltzmann Generators and Emulators

Boltzmann Generators (BGs) (Noé et al., 2019) combine exact-likelihood generative models with importance sam-

pling to obtain exact equilibrium statistics. Typically implemented using normalizing flows (Rezende & Mohamed, 2016), a BG defines a tractable proposal density $q_\theta(\mathbf{r})$ that approximates $p(\mathbf{r})$. Given samples $\mathbf{r}_i \sim q_\theta$, importance weights are assigned as

$$w(\mathbf{r}_i) = \frac{p(\mathbf{r}_i)}{q_\theta(\mathbf{r}_i)} \propto \frac{e^{-\beta u(\mathbf{r}_i)}}{q_\theta(\mathbf{r}_i)}. \quad (2)$$

Unbiased estimates of equilibrium expectations are then obtained using the self-normalized importance sampling estimator

$$\mathbb{E}_p[\mathcal{O}] \approx \frac{\sum_{i=1}^N w(\mathbf{r}_i) \mathcal{O}(\mathbf{r}_i)}{\sum_{i=1}^N w(\mathbf{r}_i)}. \quad (3)$$

Provided that q_θ overlaps sufficiently with p , this procedure converges to the exact Boltzmann average. This allows BGs to be trained on biased or non-equilibrium data, since reweighting restores equilibrium statistics at inference time.

Boltzmann Emulators adopt similar generative architectures but omit the reweighting step, estimating observables directly under q_θ . While computationally efficient at inference, emulators are no longer asymptotically exact: their accuracy depends entirely on how closely q_θ approximates $p(\mathbf{r})$. This dependence necessitates high-quality unbiased training data, whose generation is often the primary computational bottleneck.

2.2. Continuous Normalizing Flows

Continuous normalizing flows (CNFs) extend discrete normalizing flows (Rezende & Mohamed, 2016; Dinh et al., 2014) by modeling density transformations as solutions to time-dependent ordinary differential equations (ODEs) (Chen et al., 2018). A vector field $v_\theta : [0, 1] \times \mathbb{R}^n \rightarrow \mathbb{R}^n$, parameterized by a neural network, defines the dynamics

$$\frac{d\mathbf{x}(t)}{dt} = v_\theta(t, \mathbf{x}(t)), \quad \mathbf{x}(0) \sim p_0, \quad (4)$$

where p_0 is a simple prior distribution. The solution at time t is given by

$$\mathbf{x}(t) = \mathbf{x}(0) + \int_0^t v_\theta(\tau, \mathbf{x}(\tau)) d\tau. \quad (5)$$

The evolution of the log-density follows the instantaneous change-of-variables formula

$$\log p_t(\mathbf{x}(t)) = \log p_0(\mathbf{x}(0)) - \int_0^t \nabla \cdot v_\theta(\tau, \mathbf{x}(\tau)) d\tau, \quad (6)$$

where $\nabla \cdot v_\theta$ denotes the divergence of the vector field.

While CNFs are commonly trained via maximum likelihood, Flow Matching (FM) (Albergo et al., 2023; Lipman et al., 2022; Liu et al., 2022) provides a simulation-free alternative. Conditional Flow Matching (CFM) (Tong et al., 2023)

directly regresses the neural vector field v_θ onto a target conditional vector field $u_t(\mathbf{x} | z)$ that induces a prescribed probability path. The training objective is

$$\mathcal{L}_{\text{CFM}}(\theta) = \mathbb{E}_{t, z, \mathbf{x} \sim p_t(\cdot | z)} [\|v_\theta(t, \mathbf{x}) - u_t(\mathbf{x} | z)\|^2], \quad (7)$$

where $t \sim \mathcal{U}[0, 1]$ and z denotes a conditioning variable. A commonly used construction specifies the probability path through linear interpolation between paired samples (Albergo et al., 2023; Tong et al., 2023). Specifically, let $z = (\mathbf{x}_0, \mathbf{x}_1)$, where \mathbf{x}_0 and \mathbf{x}_1 are samples drawn from the source and target distributions, respectively. The interpolated state and corresponding vector field are

$$\mathbf{x}_t = (1-t)\mathbf{x}_0 + t\mathbf{x}_1, \quad u_t(\mathbf{x}_t | \mathbf{x}_0, \mathbf{x}_1) = \mathbf{x}_1 - \mathbf{x}_0. \quad (8)$$

2.3. Coarse-Graining and Potentials of Mean Force

Coarse-graining reduces dimensionality by mapping atomistic configurations $\mathbf{r} \in \mathbb{R}^n$ to a lower-dimensional set of collective variables (CVs), or *beads*, $\mathbf{R} \in \mathbb{R}^N$ ($N \ll n$), typically selected to capture the slow degrees of freedom, via a mapping $\mathbf{R} = \Xi(\mathbf{r})$. From a *bottom-up* perspective (Noid et al., 2008; Jin et al., 2022), the goal of coarse-graining is to define a suitable set of CG variables and parameterize an effective potential such that the CG model reproduces the marginal equilibrium distribution of the underlying atomistic system:

$$p(\mathbf{R}) = \int p(\mathbf{r}) \delta(\Xi(\mathbf{r}) - \mathbf{R}) d\mathbf{r}. \quad (9)$$

This marginal distribution admits a Boltzmann form,

$$p(\mathbf{R}) \propto e^{-\beta U(\mathbf{R})}, \quad (10)$$

where the effective energy $U(\mathbf{R})$, known as the *potential of mean force*, is defined up to an additive constant as

$$U(\mathbf{R}) = -k_B T \ln \int e^{-\beta u(\mathbf{r})} \delta(\Xi(\mathbf{r}) - \mathbf{R}) d\mathbf{r}. \quad (11)$$

The PMF captures both energetic and entropic contributions from the eliminated degrees of freedom and generally induces many-body, state-dependent interactions (Krishna et al., 2009).

In practice, the PMF is intractable due to the high-dimensional integral over \mathbf{r} . Classical CG force fields (Marrink et al., 2007; Souza et al., 2021) approximate $U(\mathbf{R})$ using fixed functional forms, which may lack sufficient expressivity. Recent approaches parameterize $U(\mathbf{R})$ using neural networks trained via variational principles such as force matching (Noid et al., 2008; Wang et al., 2019) or relative entropy minimization (Shell, 2008; Thaler et al., 2022).

3. Coarse-Grained Boltzmann Generators

Atomistic BGs provide exact equilibrium sampling but scale poorly to large systems, while CG Boltzmann Emulators improve scalability at the cost of persistent bias due to the absence of reweighting.

We propose CG-BGs that reconcile scalability with statistical rigor by performing generative modeling and importance sampling directly in CG coordinate space. Rather than targeting the full atomistic distribution, CG-BGs target the marginal distribution $p(\mathbf{R})$ defined by the PMF.

CG-BGs have two major components: a flow-based generative model to propose CG samples (similar to atomistic BGs) and a machine learning PMF acting as an energy predictor for importance sampling. Unlike atomistic MLPs trained on potential energy surfaces (Behler & Parrinello, 2007; Blank et al., 1995), CG MLPs have no ground-truth energy labels, since the PMF is a free energy that includes entropic contributions from eliminated degrees of freedom. We next describe how the PMF is learned from atomistic simulations and outline the CG-BG workflow (Fig. 1).

3.1. Variational Force Matching

Variational Force Matching (VFM) (Noid et al., 2008), also known as multiscale coarse-graining, is a bottom-up approach for learning the PMF from atomistic forces.

The central premise is that the CG forces predicted by the model should match, on average, the instantaneous atomistic forces projected onto the CG coordinates, denoted as $\mathcal{F}_{\text{proj}}(\mathbf{r})$. The gradient of the exact PMF satisfies:

$$-\nabla U(\mathbf{R}) = \mathbb{E}_{p(\mathbf{r}|\mathbf{R})} [\mathcal{F}_{\text{proj}}(\mathbf{r})]. \quad (12)$$

where the expectation is taken over the *fiber distribution* (Hummerich et al., 2025), i.e., the conditional probability of a fine-grained configuration \mathbf{r} given its CG representative \mathbf{R} .

From a learning perspective, instantaneous projected forces provide noisy samples to approximate the target mean force. Given a dataset \mathcal{D} of atomistic configurations, a parameterized CG potential $U_\eta(\mathbf{R})$ is trained by minimizing

$$\mathcal{L}_{\text{VFM}}(\eta) = \mathbb{E}_{\mathbf{r} \sim \mathcal{D}} \left[\left\| \nabla_{\mathbf{R}} U_\eta(\Xi(\mathbf{r})) + \mathcal{F}_{\text{proj}}(\mathbf{r}) \right\|_2^2 \right]. \quad (13)$$

When \mathcal{D} is sampled from equilibrium, this objective minimizes the Fisher divergence between the model distribution $p_\eta(\mathbf{R})$ and the true marginal $p(\mathbf{R})$. Theoretical error bounds follow from Log-Sobolev inequalities (Proof in §A.1):

Proposition 1. *Let $p^*(\mathbf{R}) \propto e^{-\beta U^*(\mathbf{R})}$ be the true marginal and $p_\eta(\mathbf{R}) \propto e^{-\beta U_\eta(\mathbf{R})}$ the learned distribution. If p^* satisfies a Logarithmic Sobolev Inequality (LSI) with constant $\rho > 0$. Then, the Kullback-Leibler*

divergence between the learned and true distributions is bounded by the expected squared force error:

$$\mathcal{D}_{\text{KL}}(p_\eta \| p^*) \leq \frac{\beta^2}{2\rho} \mathbb{E}_{p_\eta} [\|\nabla U_\eta(\mathbf{R}) - \nabla U^*(\mathbf{R})\|^2]. \quad (14)$$

While global LSI conditions are strong assumptions for multimodal PMFs (Vempala & Wibisono, 2019), this proposition theoretically motivates minimizing force errors as a proxy for distributional accuracy. This is important for the subsequent importance sampling step, as the quality of the reweighted ensemble depends directly on the divergence between the learned target and the true marginal.

3.2. Enhanced Sampling for Force Matching

Standard force matching relies on unbiased equilibrium data, which can be prohibitively expensive to obtain for systems with metastable states and large free-energy barriers—a limitation shared by Boltzmann Emulators. Moreover, the Boltzmann distribution decays exponentially with energy, leading to sparse sampling of high-energy transition regions that are critical for accurately reconstructing the global PMF.

Enhanced sampling force matching (ESFM) (Chen et al., 2026) overcomes these limitations by exploiting the invariance of the fiber (conditional) distribution under coarse-grained biasing.

Proposition 2. (Chen et al. (2026)) *Let $V(\mathbf{R})$ be a bias potential depending only on the coarse-grained coordinates. The conditional distribution of atomistic configurations given \mathbf{R} remains unchanged:*

$$p_V(\mathbf{r} | \mathbf{R}) = p(\mathbf{r} | \mathbf{R}). \quad (15)$$

Since the mean force $-\nabla U(\mathbf{R})$ is the expectation of the projected forces over this conditional distribution (Eq. 12), the force regression targets remain unbiased even when sampled from a biased equilibrium ensemble. ESFM therefore minimizes

$$\mathcal{L}_{\text{ESFM}}(\eta) = \mathbb{E}_{\mathbf{r} \sim \mathcal{D}_{\text{bias}}} \left[\left\| \nabla_{\mathbf{R}} U_\eta(\Xi(\mathbf{r})) + \mathcal{F}_{\text{proj}}(\mathbf{r}) \right\|_2^2 \right], \quad (16)$$

where $\mathcal{D}_{\text{bias}}$ is a rapidly converged dataset generated via enhanced sampling and $\mathcal{F}_{\text{proj}}(\mathbf{r})$ denotes forces recomputed using the unbiased atomistic potential.

Proposition 3. (Chen et al. (2026)) *Minimizing $\mathcal{L}_{\text{ESFM}}$ yields the same global optimum as standard force matching loss \mathcal{L}_{VFM} , assuming sufficient model expressivity.*

Together, Propositions 2 (Proof in §A.2) and 3 establish that ESFM enables accurate PMF learning from rapidly converged data, benefiting from faster convergence and improved coverage of transition regions.

3.3. The CG-BG Workflow

After training, the learned PMF U_η defines the target energy for importance sampling, rather than serving as a force field for MD integration. Let $q_\theta(\mathbf{R})$ denote the density induced by the trained flow model. Importance weights are computed as

$$w(\mathbf{R}) \propto \frac{\exp(-\beta U_\eta(\mathbf{R}))}{q_\theta(\mathbf{R})}. \quad (17)$$

Provided U_η accurately approximates the true PMF on the support of q_θ , this procedure gives unbiased estimates under $p(\mathbf{R})$.

The reliability of importance reweighting is quantified by the effective sample size (ESS) (Kish, 1965),

$$\text{ESS} = \frac{\left(\sum_{i=1}^B w(\mathbf{R}_i)\right)^2}{\sum_{i=1}^B w(\mathbf{R}_i)^2}. \quad (18)$$

The ESS depends critically on the overlap between the generative density q_θ and the target density defined by U_η . In practice, machine learning potentials may exhibit unphysical extrapolation outside the training domain, and generative models may occasionally produce high-energy artifacts, both of which can lead to weight degeneracy. To improve robustness, we apply a weight clipping strategy (Tan et al., 2025a; Gloy & Olsson, 2025; Moqvist et al., 2025) to truncate statistical outliers before computing expectations (See §G.2). The complete CG-BG training and sampling pipeline is summarized in Fig. 1.

4. Experiments

We evaluate CG-BGs on the Müller–Brown (MB) potential and alanine dipeptide (capped alanine). Additional experimental details including architectures are provided in §C and §D. CG-BG samples are generated and reweighted following the algorithms described in §F.

Datasets. For both systems, we construct unbiased and biased datasets for training and evaluation. Biased datasets are generated using enhanced sampling methods to accelerate exploration of configurational space. For the MB system, datasets are generated via Langevin dynamics (§B.1), with umbrella sampling (Torrie & Valleau, 1977) applied in the biased setting to facilitate transitions between metastable basins. For alanine dipeptide, we generate datasets using both explicit and implicit solvent models (§B.2). Explicit solvent datasets, used for training, are produced using a classical force field (Lindorff-Larsen et al., 2010) and include long unbiased trajectories as well as biased simulations from well-tempered metadynamics (Barducci et al., 2008). Implicit solvent datasets are generated with the same force field combined with a generalized Born solvent model, using

two parameterizations (OBC1 and OBC2) (Onufriev et al., 2004). The explicit solvent trajectories are further coarse-grained using either a *Heavy Atom* mapping (Fig. 3a), which retains all heavy atoms, or a *Core Beta* mapping (Fig. 4a), which preserves the backbone and C_β atoms. Full details on dataset generation and enhanced sampling procedures are provided in §B.

Baselines. Unlike previous BG work (Klein & Noé, 2024; Tan et al., 2025a;b), which often treats implicit solvent simulations as ground truth, we use explicit solvent simulations as reference and regard implicit solvent models as baselines. For alanine dipeptide, CG reduces the effective dimensionality to either 10 beads (Heavy Atom) or 6 beads (Core Beta). To quantify the computational gain via coarse-graining, we use the full 22-atom system as a baseline.

Metrics. We report ESS, Jenson–Shannon (JS) divergence, and PMF error. JS divergence is computed between the sampled and reference dihedral angle free energy profiles. The PMF error is defined as the squared distance between the negative logarithms of the sampled and reference densities, which gives more weight to low-density regions compared to JS divergence (Plainer et al., 2025; Durumeric et al., 2024). Energy histograms and free energy profiles of ϕ dihedral are shown in the main text, while additional results, including ψ dihedral free energy profiles, Ramachandran plots (Ramachandran, 1963), bond length distributions, and weight clipping ablations, are provided in §G.

4.1. Recovering Equilibrium Distributions from Biased and Unbiased Data

We first demonstrate that CG-BGs inherit the importance reweighting capability of atomistic BGs, enabling recovery of unbiased equilibrium statistics from flow models trained on either biased or unbiased trajectories.

For the MB system (Fig. 2a–b), coarse-graining corresponds to projection onto the x -coordinate, yielding an analytically exact reference $U(x) = -k_B T \ln \int \exp(-\beta u(x, y)) dy$ (Fig. 2c–d). For alanine dipeptide, we use the Heavy Atom mapping, which removes hydrogens and solvent degrees of freedom (Fig. 3a). Throughout §4.1 and §4.2, the PMF is learned from rapidly converged datasets using ESFM (§3.2).

As shown in Fig. 2c and Fig. 3c, despite training on long unbiased datasets and using highly expressive models, the raw flow proposals deviate from the MD reference. These discrepancies arise from low-quality samples generated by the flow model, a limitation intrinsic to Boltzmann Emulators that cannot be systematically corrected without reweighting. After reweighting, however, CG-BGs successfully recover equilibrium free energy profiles in close agreement with MD references (Fig. 2c and Fig. 3b–c). The reweighted distributions accurately reproduce relative basin populations and

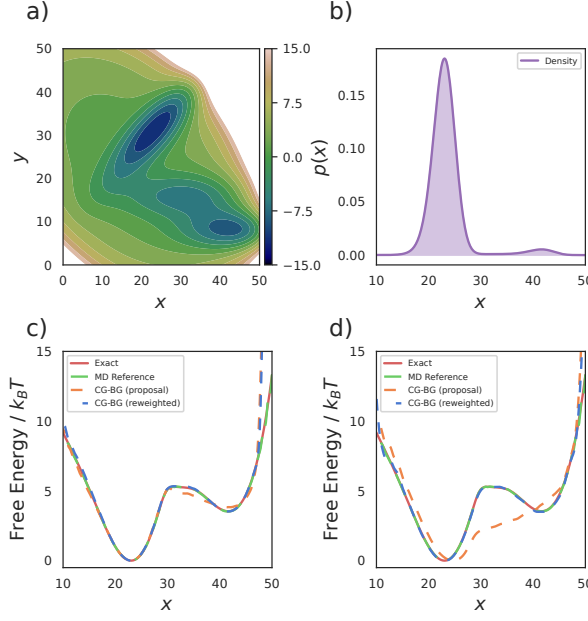


Figure 2. CG-BGs on the MB potential. (a) Two-dimensional MB potential energy surface (functional form in §B). (b) Marginal probability density along the x coordinate. (c) Free energy profiles before and after reweighting for CG-BGs, where flow is trained on *unbiased* data, compared with the exact solution and MD reference. (d) Same as (c), but for flow trained on *biased* data.

capture transition regions. This is further illustrated by the Ramachandran plots (Fig. 7). Unreweighted proposals exhibit noisy samples across transition regions and metastable basins (Fig. 7b), which are assigned low importance weights and effectively filtered out after reweighting (Fig. 7c). Quantitative metrics in Tab. 2 confirm close agreement between reweighted samples and target equilibrium ensemble.

We further evaluate CG-BGs trained on biased or short non-equilibrium trajectories (umbrella sampling for MB and 10 ns WT-MetaD with $\gamma = 1.5$ for alanine dipeptide), reflecting realistic settings where long unbiased simulations are infeasible. As shown in Fig. 2d, Fig. 3d and Fig. 7c, while the flow proposals exhibit larger deviations from the MD reference, importance reweighting consistently recovers accurate equilibrium statistics (Tab. 2).

Notably, after reweighting, CG-BGs outperform implicit solvent MD baselines (Tab. 2), highlighting the advantage of learning PMFs from explicit solvent simulations. While implicit solvent models perform reasonably well for alanine dipeptide, prior work has reported drastic discrepancies for more complex systems (Chen et al., 2021). This constitutes an improvement over previous BG approaches, which rely on implicit solvent models for reweighting and are therefore fundamentally limited by solvent approximation error. In other words, such models can at best achieve the accuracy of implicit solvent baselines (Tab. 2). These results show that

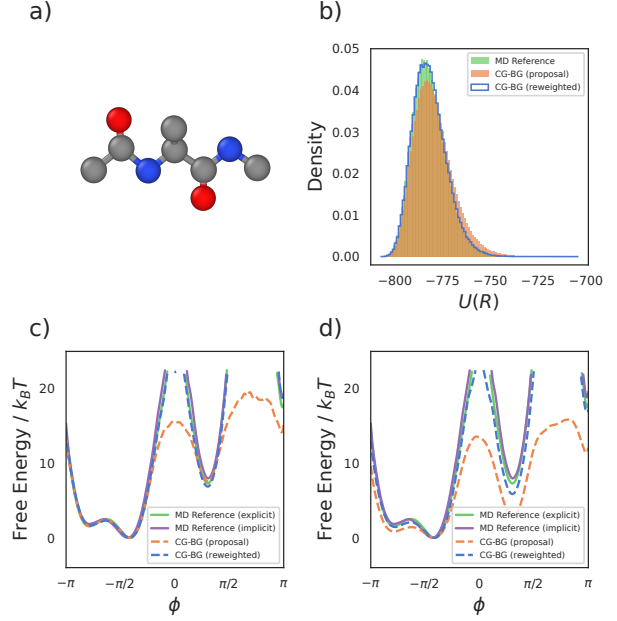


Figure 3. CG-BGs on alanine dipeptide (Heavy Atom). (a) Heavy Atom mapping. (b) Potential energy distributions under the learned PMF before and after reweighting, compared with the MD reference. (c) ϕ dihedral free energy profile before and after reweighting for CG-BGs, where flow is trained on 500 ns *unbiased* data, alongside the MD reference. (d) Same as (c), but for flow trained on a 10 ns *WT-MetaD* ($\gamma = 1.5$) dataset.

CG-BGs generate CG equilibrium samples consistent with the target distribution, without requiring long unbiased MD simulations, and offer a practical route to correct systematic biases in existing Boltzmann Emulators.

4.2. Effect of Coarse-Graining Resolution on Accuracy and Efficiency

We next examine how the choice of CG resolution affects both modeling accuracy and computational efficiency. To this end, we consider a coarser representation of alanine dipeptide, the Core Beta mapping (Fig. 4a).

Despite the reduced resolution, CG-BGs trained with the Core Beta mapping remain capable of recovering equilibrium statistics after reweighting (Fig. 4c–d and Fig. 10), with quantitative metrics reported in Tab. 2. While performance remains strong for alanine dipeptide, coarser mappings are known to induce a gradual loss of accuracy for more complex systems (Görlich & Zavadlav, 2025). This degradation arises from increased degeneracy in the CG representation. For a given CG coordinate \mathbf{R} , many atomistic microstates \mathbf{r}_i satisfy $\Xi(\mathbf{r}_i) = \mathbf{R}$ while exerting different projected forces $\mathcal{F}_{\text{proj}}(\mathbf{r}_i)$. As a result, the conditional mean force $\mathbb{E}_{p(\mathbf{r}|\mathbf{R})}[\mathcal{F}_{\text{proj}}(\mathbf{r})]$ exhibits higher variance under coarser mappings, introducing irreducible uncertainty and making the force matching problem intrinsically more challenging.

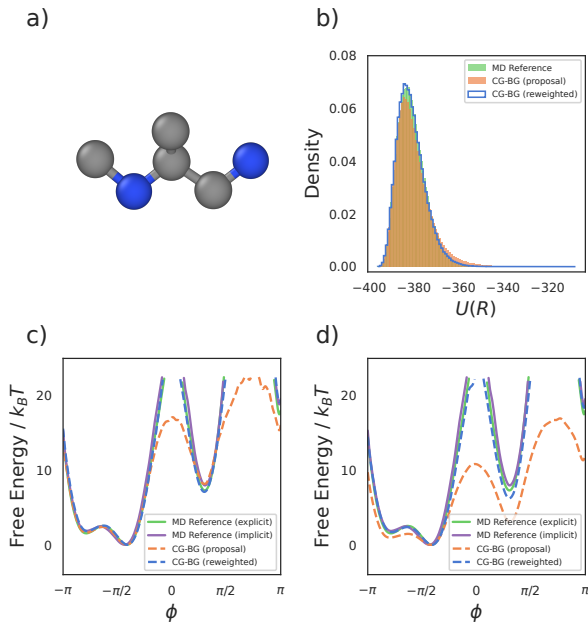


Figure 4. CG-BGs on alanine dipeptide (Core Beta). (a) Core Beta mapping. (b) Potential energy distributions under the learned PMF before and after reweighting, compared with the MD reference. (c) ϕ dihedral free energy profile before and after reweighting for CG-BGs, where flow is trained on 500 ns *unbiased* data, alongside the MD reference. (d) Same as (c), but for flow trained on a 10 ns *WT-MetaD* ($\gamma = 1.5$) dataset.

We further benchmark the computational cost of CG-BGs across different resolutions (Tab. 1). As expected, the Core Beta mapping substantially reduces both training and inference time compared to the Heavy Atom and full atomistic representations, with particularly large gains at inference due to cheaper Jacobian evaluations. Note that the reported all atom baseline generates only solute coordinates; generating full configurations with explicit solvent, which would be the proper reference, is computationally infeasible. Overall, these results highlight the favorable accuracy–efficiency trade-off of CG-BGs. Additional comparisons with prior work are provided in Tab. 4.

4.3. Simulation-Free Evaluation of Learned PMFs

Beyond equilibrium sampling, CG-BGs also provide a practical tool for evaluating learned PMFs without running MD.

Table 1. Training and inference time across different CG mappings. Inference times correspond to 10^4 generated samples. *All Atom* denotes generating the full solute configuration without solvent.

Stage	Core Beta	Heavy Atom	All Atom
Training	0.83h	1.39h	3.93h
Inference	0.84min	3.46min	13.92min
Total	0.84h	1.45h	4.16h

The flow model generates CG configurations from a proposal distribution approximating the equilibrium ensemble, and importance reweighting maps these samples to the Boltzmann distribution induced by a given PMF. As a result, equilibrium observables for any candidate PMF can be estimated using a single set of generated samples and associated weights, without additional simulations. In contrast to traditional validation pipelines that require long MD runs for each model, CG-BGs enable rapid, one-shot benchmarking of CG potentials.

We leverage this capability to benchmark PMFs trained under different data regimes, comparing models learned from long unbiased MD trajectories (PMF_U) with those trained on a rapidly converged biased dataset (PMF_B). Quantitative metrics (Tab. 2) computed from reweighted samples provide immediate feedback on model accuracy, while visual diagnostics including probability densities (Fig. 5a), dihedral free energy profiles (Fig. 5b), and Ramachandran plots (Fig. 9) qualitative validation against atomistic references. Consistent with prior observations (Chen et al., 2026; Görlich & Zavadlav, 2025), PMF_U fails to capture the correct metastable population of the ϕ angle, whereas PMF_B shows improved agreement.

While demonstrated here for CG models, this simulation-free evaluation paradigm naturally extends to atomistic MLPs. CG-BGs therefore serve not only as efficient equilibrium sampling methods, but also as diagnostic tools for rapid comparison and validation of learned energy models.

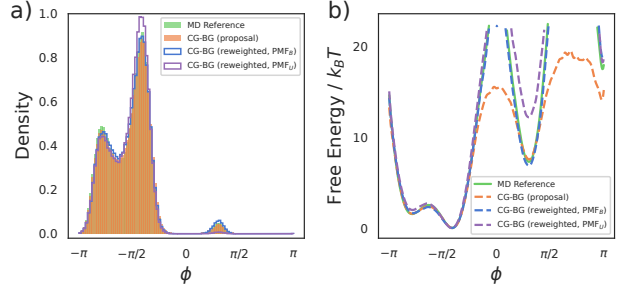


Figure 5. Simulation-free benchmarking of learned CG PMFs using CG-BGs (Heavy Atom). (a) Probability density of the ϕ dihedral angle after reweighting with PMFs trained on unbiased (PMF_U) and rapidly converged biased datasets (PMF_B), compared with the MD reference and flow proposal (trained on unbiased data). (b) Corresponding ϕ dihedral free energy profiles after reweighting, alongside the MD reference and flow proposal.

5. Related Work

Generative models for equilibrium molecular sampling. Generative models have emerged as powerful tools for sampling Boltzmann distributions (Olsson, 2026; Klein et al., 2023; Rotskoff, 2024; Aranganathan et al., 2025; Janson & Feig, 2025). In particular, Boltzmann Generators (Noé

Table 2. Quantitative comparison for alanine dipeptide across CG resolutions and baseline models. CG-BGs results are reported after reweighting; *Biased* denotes flow trained on WT-MetaD datasets, while PMF_U indicates PMFs learned from long unbiased MD data.

Model	JS (↓)	PMF (↓)	ESS (↑)
CG-BGs (Reweighted)			
Heavy Atom	0.0075 ± 0.0001	0.2493 ± 0.0126	0.2325 ± 0.0006
Heavy Atom (Biased)	0.0090 ± 0.0002	0.2758 ± 0.0109	0.1936 ± 0.0005
Core Beta	0.0079 ± 0.0001	0.2519 ± 0.0136	0.2510 ± 0.0006
Core Beta (Biased)	0.0081 ± 0.0001	0.2325 ± 0.0093	0.2239 ± 0.0005
Heavy Atom (PMF_U)	0.0218 ± 0.0002	0.3611 ± 0.0138	0.2222 ± 0.0006
Implicit Solvent Baselines (Generalized Born Models)			
GB (OBC1)	0.0157 ± 0.0002	0.3709 ± 0.0092	–
GB (OBC2)	0.0182 ± 0.0002	0.4028 ± 0.0095	–

et al., 2019) represent an influential class of such models. Subsequent work has improved BGs in various ways (von Klitzing et al., 2025; Schebek & Rogal, 2025), including incorporating inductive biases (Köhler et al., 2020) and enhancing transferability across chemical and thermodynamic conditions (Klein & Noé, 2024; Dibak et al., 2022; Moqvist et al., 2025; Invernizzi et al., 2022). Despite efforts to employ scalable architectures (Tan et al., 2025a; Zhai et al., 2024) or reduce the cost of likelihood evaluation (Gloy & Olsson, 2025; Rehman et al., 2025; Peng & Gao, 2025), atomistic BGs remain limited in scalability. CG Boltzmann Emulators (Lewis et al., 2025; Zheng et al., 2024) bypass the reweighting step, enabling larger-scale applications at the cost of asymptotic exactness. To bridge the resolution gap, backmapping (Chennakesavalu et al., 2023; Hummerich et al., 2025; Wang et al., 2022) or other reconstruction strategies (Tamagnone et al., 2024; Schopmans & Friederich, 2024; Stupp & Koutsourelakis, 2025) are often employed to recover atomistic detail. Another active line of research considers neural samplers for sampling unnormalized densities (Akhound-Sadegh et al., 2024; Midgley et al., 2023; He et al., 2025; Potapchik et al., 2025; Liu et al., 2025), which also have applications in molecular systems (Nam et al., 2025; Havens et al., 2025).

Coarse-grained machine learning potentials. CG potentials have historically been parameterized using either *top-down* or *bottom-up* approaches. In top-down methods, model parameters are adjusted to reproduce macroscopic observables, such as experimental measurements (Marrink et al., 2007; Thaler & Zavadlav, 2021; Fuchs & Zavadlav, 2025). In contrast, bottom-up approaches aim to construct CG models that reproduce the marginal equilibrium distribution or free energy landscape of the underlying atomistic system (Jin et al., 2022; Noid, 2013). Prominent bottom-up methods include variational force matching (Noid et al., 2008) and relative entropy minimization (Shell, 2008). Recent progress in machine learning has opened new opportunities for learning CG MLPs (Plainer et al., 2025; Kohler

et al., 2023; Arts et al., 2023; Wang et al., 2019; Zhang et al., 2018). The development of CG MLPs can be viewed as an extension of broader effort to construct accurate machine learning interatomic potentials from first-principles calculations. (Batazia et al., 2022; Wood et al., 2025; Batzner et al., 2022; Unke et al., 2021; Kabylda et al., 2025). Despite these successes, learning transferable and efficient CG MLPs remains an open challenge (Charron et al., 2025; Mirarchi et al., 2024; Majewski et al., 2023; Durumeric et al., 2023).

6. Conclusion

This work introduces CG-BGs, a scalable framework for equilibrium sampling of coarse-grained molecular systems. By targeting the marginal equilibrium distribution defined by the PMF, CG-BGs reduce the effective dimensionality of the sampling problem while preserving thermodynamic consistency through importance reweighting. The underlying PMF can be learned from rapidly converged data using enhanced sampling force matching, providing a correction mechanism for existing CG Boltzmann Emulators. Even at high levels of coarse-graining, CG-BGs capture solvent-mediated and many-body effects, and enable one-shot, simulation-free evaluation of CG MLPs.

Limitations. The current approach relies on predefined collective variables for coarse-graining and enhanced sampling, which may be nontrivial to identify for complex systems. Recent advances in collective variable discovery (Zhang et al., 2024; Ribeiro et al., 2018; Chen & Ferguson, 2018; Herringer et al., 2023; Mehdi et al., 2024) and uncertainty quantification (Zaverkin et al., 2024; Musil et al., 2019) provide promising avenues to address these challenges.

Future work. Extending CG-BGs to larger, more complex systems is a natural next step, leveraging demonstrated transferability of flow-based generative models and MLPs. The simulation-free evaluation paradigm introduced here also opens new opportunities, including integrating CG-BGs with experimental data by incorporating it into the

learned PMF, and accelerating differentiable training strategies (Thaler & Zavadlav, 2021; Han & Yu, 2025) by replacing iterative simulations with high-quality generated samples.

Broader Impact

This work focuses on sampling from Boltzmann distributions, a problem of broad interest in machine learning and AI for Science, with applications in both statistical physics and molecular simulations. We introduce Coarse-Grained Boltzmann Generators, which can be trained on molecular systems and applied to tasks such as drug and material discovery. While we do not anticipate immediate negative impacts, we encourage careful consideration when scaling these methods to prevent potential misuse.

Acknowledgements

We thank Simon Olsson, Franz Görlich, Nuno Costa, and Paul Fuchs for fruitful discussions and helpful feedback. This work was funded by the European Union through the ERC (StG SupraModel) - 101077842. Views and opinions expressed are however those of the author(s) only and do not necessarily reflect those of the European Union or the European Research Council Executive Agency. Neither the European Union nor the granting authority can be held responsible for them.

References

Abramson, J., Adler, J., Dunger, J., Evans, R., Green, T., Pritzel, A., Ronneberger, O., Willmore, L., Ballard, A. J., Bambrick, J., et al. Accurate structure prediction of biomolecular interactions with alphafold 3. *Nature*, pp. 1–3, 2024.

Akhound-Sadegh, T., Rector-Brooks, J., Bose, A. J., Mittal, S., Lemos, P., Liu, C.-H., Sendera, M., Ravanbakhsh, S., Gidel, G., Bengio, Y., et al. Iterated denoising energy matching for sampling from boltzmann densities. *arXiv preprint arXiv:2402.06121*, 2024.

Albergo, M. S., Kanwar, G., and Shanahan, P. E. Flow-based generative models for markov chain monte carlo in lattice field theory. *Physical Review D*, 100(3):034515, 2019.

Albergo, M. S., Boffi, N. M., and Vanden-Eijnden, E. Stochastic interpolants: A unifying framework for flows and diffusions. *arXiv preprint arXiv:2303.08797*, 2023.

Aranganathan, A., Gu, X., Wang, D., Vani, B. P., and Tiwary, P. Modeling boltzmann-weighted structural ensembles of proteins using artificial intelligence-based methods. *Current opinion in structural biology*, 91:103000, 2025.

Arts, M., Garcia Satorras, V., Huang, C.-W., Zügner, D., Federici, M., Clementi, C., Noé, F., Pinsler, R., and van den Berg, R. Two for One: Diffusion Models and Force Fields for Coarse-Grained Molecular Dynamics. *Journal of Chemical Theory and Computation*, 19(18): 6151–6159, September 2023. ISSN 1549-9618. doi: 10.1021/acs.jctc.3c00702.

Barducci, A., Bussi, G., and Parrinello, M. Well-tempered metadynamics: a smoothly converging and tunable free-energy method. *Physical review letters*, 100(2):020603, 2008.

Batatia, I., Kovacs, D. P., Simm, G., Ortner, C., and Csányi, G. Mace: Higher order equivariant message passing neural networks for fast and accurate force fields. *Advances in neural information processing systems*, 35: 11423–11436, 2022.

Batzner, S., Musaelian, A., Sun, L., Geiger, M., Mailoa, J. P., Kornbluth, M., Molinari, N., Smidt, T. E., and Kozinsky, B. E (3)-equivariant graph neural networks for data-efficient and accurate interatomic potentials. *Nature communications*, 13(1):2453, 2022.

Behler, J. and Parrinello, M. Generalized neural-network representation of high-dimensional potential-energy surfaces. *Physical review letters*, 98(14):146401, 2007.

Blank, T. B., Brown, S. D., Calhoun, A. W., and Doren, D. J. Neural network models of potential energy surfaces. *The Journal of chemical physics*, 103(10):4129–4137, 1995.

Bonomi, M., Branduardi, D., Bussi, G., Camilloni, C., Provasi, D., Raiteri, P., Donadio, D., Marinelli, F., Pietrucci, F., Broglia, R. A., et al. Plumed: A portable plugin for free-energy calculations with molecular dynamics. *Computer Physics Communications*, 180(10): 1961–1972, 2009.

Chandler, D. *Introduction to Modern Statistical Mechanics*. Oxford University Press, 1987.

Charron, N. E., Bonneau, K., Pasos-Trejo, A. S., Guljas, A., Chen, Y., Musil, F., Venturin, J., Gusew, D., Zaporozhets, I., Krämer, A., et al. Navigating protein landscapes with a machine-learned transferable coarse-grained model. *Nature Chemistry*, pp. 1–9, 2025.

Chen, R. T., Rubanova, Y., Bettencourt, J., and Duvenaud, D. K. Neural ordinary differential equations. *Advances in neural information processing systems*, 31, 2018.

Chen, W. and Ferguson, A. L. Molecular enhanced sampling with autoencoders: On-the-fly collective variable discovery and accelerated free energy landscape exploration. *Journal of computational chemistry*, 39(25):2079–2102, 2018.

Chen, W., Görlich, F., Fuchs, P., and Zavadlav, J. Enhanced sampling for efficient learning of coarse-grained machine learning potentials. *Journal of Chemical Theory and Computation*, 22(1):219–230, 2026. doi: 10.1021/acs.jctc.5c01712. URL <https://doi.org/10.1021/acs.jctc.5c01712>.

Chen, Y., Krämer, A., Charron, N. E., Husic, B. E., Clementi, C., and Noé, F. Machine learning implicit solvation for molecular dynamics. *The Journal of Chemical Physics*, 155(8):084101, August 2021. ISSN 1089-7690. doi: 10.1063/5.0059915. URL <http://dx.doi.org/10.1063/5.0059915>.

Chennakesavalu, S., Toomer, D. J., and Rotskoff, G. M. Ensuring thermodynamic consistency with invertible coarse-graining. *The Journal of Chemical Physics*, 158(12), 2023.

Chipot, C. and Pohorille, A. *Free energy calculations*, volume 86. Springer, 2007.

Costa, A. d. S., Ponnappati, M., Rubin, D., Smidt, T., and Jacobson, J. Accelerating protein molecular dynamics simulation with deepjump. *arXiv preprint arXiv:2509.13294*, 2025.

Daigavane, A., Vani, B. P., Davidson, D., Saremi, S., Rackers, J. A., and Kleinhenz, J. Jamun: Bridging smoothed molecular dynamics and score-based learning for conformational ensemble generation. In *The Thirty-ninth Annual Conference on Neural Information Processing Systems*, 2025.

Dibak, M., Klein, L., Krämer, A., and Noé, F. Temperature steerable flows and boltzmann generators, 2022. URL <https://arxiv.org/abs/2108.01590>.

Diez, J. V., Schreiner, M., and Olsson, S. Transferable generative models bridge femtosecond to nanosecond time-step molecular dynamics. *arXiv preprint arXiv:2510.07589*, 2025.

Dinh, L., Krueger, D., and Bengio, Y. Nice: Non-linear independent components estimation. *arXiv preprint arXiv:1410.8516*, 2014.

dos Santos Costa, A., Mitnikov, I., Pellegrini, F., Daigavane, A., Geiger, M., Cao, Z., Kreis, K., Smidt, T., Kucukbenli, E., and Jacobson, J. Equijump: Protein dynamics simulation via $so(3)$ -equivariant stochastic interpolants, 2024.

Durumeric, A. E., Chen, Y., Noé, F., and Clementi, C. Learning data efficient coarse-grained molecular dynamics from forces and noise. *arXiv preprint arXiv:2407.01286*, 2024.

Durumeric, A. E. P., Charron, N. E., Templeton, C., Musil, F., Bonneau, K., Pasos-Trejo, A. S., Chen, Y., Kelkar, A., Noé, F., and Clementi, C. Machine learned coarse-grained protein force-fields: Are we there yet? *Current Opinion in Structural Biology*, 79:102533, April 2023. ISSN 0959-440X. doi: 10.1016/j.sbi.2023.102533.

Eastman, P., Galvelis, R., Peláez, R. P., Abreu, C. R., Farr, S. E., Gallicchio, E., Gorenko, A., Henry, M. M., Hu, F., Huang, J., et al. Openmm 8: molecular dynamics simulation with machine learning potentials. *The Journal of Physical Chemistry B*, 128(1):109–116, 2023.

Frenkel, D. and Smit, B. *Understanding Molecular Simulation*. Elsevier, 2002. doi: 10.1016/b978-0-12-267351-1.x5000-7. URL <https://doi.org/10.1016/b978-0-12-267351-1.x5000-7>.

Fuchs, P. and Zavadlav, J. Refining machine learning potentials through thermodynamic theory of phase transitions. *arXiv preprint arXiv:2512.03974*, 2025.

Fuchs, P., Chen, W., Thaler, S., and Zavadlav, J. chemtrain-deploy: A parallel and scalable framework for machine learning potentials in million-atom md simulations. *Journal of Chemical Theory and Computation*, 21(15):7550–7560, 2025a.

Fuchs, P., Thaler, S., Röcken, S., and Zavadlav, J. chemtrain: Learning deep potential models via automatic differentiation and statistical physics. *Computer Physics Communications*, 310:109512, 2025b.

Gloy, J. F. and Olsson, S. Hollowflow: Efficient sample likelihood evaluation using hollow message passing. *arXiv preprint arXiv:2510.21542*, 2025.

Görlich, F. and Zavadlav, J. Mapping still matters: Coarse-graining with machine learning potentials. *arXiv preprint arXiv:2512.07692*, 2025.

Han, B. and Yu, K. Refining potential energy surface through dynamical properties via differentiable molecular simulation. *Nature Communications*, 16(1):816, 2025.

Havens, A., Miller, B. K., Yan, B., Domingo-Enrich, C., Sriram, A., Wood, B., Levine, D., Hu, B., Amos, B., Karrer, B., et al. Adjoint sampling: Highly scalable diffusion samplers via adjoint matching. *arXiv preprint arXiv:2504.11713*, 2025.

Hawkins, G. D., Cramer, C. J., and Truhlar, D. G. Pairwise solute descreening of solute charges from a dielectric medium. *Chemical Physics Letters*, 246(1-2):122–129, 1995.

He, J., Du, Y., Vargas, F., Zhang, D., Padhy, S., OuYang, R., Gomes, C., and Hernández-Lobato, J. M. No trick,

no treat: Pursuits and challenges towards simulation-free training of neural samplers. *arXiv preprint arXiv:2502.06685*, 2025.

Heek, J., Levskaya, A., Oliver, A., Ritter, M., Rondepierre, B., Steiner, A., and van Zee, M. Flax: A neural network library and ecosystem for JAX, 2024. URL <http://github.com/google/flax>.

Hénin, J., Lelièvre, T., Shirts, M. R., Valsson, O., and Delemonette, L. Enhanced sampling methods for molecular dynamics simulations [article v1.0]. *Living Journal of Computational Molecular Science*, 4(1), 2022. doi: 10.33011/livecoms.4.1.1583. URL <https://doi.org/10.33011/livecoms.4.1.1583>.

Herringer, N. S., Dasetty, S., Gandhi, D., Lee, J., and Ferguson, A. L. Permutationally invariant networks for enhanced sampling (pines): Discovery of multimolecular and solvent-inclusive collective variables. *Journal of Chemical Theory and Computation*, 20(1):178–198, 2023.

Hummerich, S., Bereau, T., and Köthe, U. Split-flows: Measure transport and information loss across molecular resolutions. *arXiv preprint arXiv:2511.01464*, 2025.

Hutchinson, M. F. A stochastic estimator of the trace of the influence matrix for laplacian smoothing splines. *Communications in Statistics-Simulation and Computation*, 18(3):1059–1076, 1989.

Invernizzi, M., Kramer, A., Clementi, C., and Noé, F. Skipping the replica exchange ladder with normalizing flows. *The Journal of Physical Chemistry Letters*, 13(50):11643–11649, 2022.

Janson, G. and Feig, M. Generation of protein dynamics by machine learning. *Current Opinion in Structural Biology*, 93:103115, 2025.

Jin, J., Pak, A. J., Durumeric, A. E. P., Loose, T. D., and Voth, G. A. Bottom-up Coarse-Graining: Principles and Perspectives. *Journal of Chemical Theory and Computation*, 18(10):5759–5791, October 2022. ISSN 1549-9618. doi: 10.1021/acs.jctc.2c00643.

Jing, B., Berger, B., and Jaakkola, T. Alphafold meets flow matching for generating protein ensembles. *arXiv preprint arXiv:2402.04845*, 2024.

Kabylda, A., Frank, J. T., Suárez-Dou, S., Khabibrakhmanov, A., Medrano Sandonas, L., Unke, O. T., Chmiela, S., Müller, K.-R., and Tkatchenko, A. Molecular simulations with a pretrained neural network and universal pairwise force fields. *Journal of the American Chemical Society*, 147(37):33723–33734, 2025.

Kidger, P. *On Neural Differential Equations*. PhD thesis, University of Oxford, 2021.

Kish, L. *Survey Sampling*. John Wiley & Sons, Inc, New York, 1965.

Klein, L. and Noé, F. Transferable boltzmann generators. *Advances in Neural Information Processing Systems*, 37: 45281–45314, 2024.

Klein, L., Foong, A. Y. K., Fjelde, T. E., Mlodzeniec, B., Brockschmidt, M., Nowozin, S., Noé, F., and Tomioka, R. Timewarp: Transferable acceleration of molecular dynamics by learning time-coarsened dynamics, 2023. URL <https://arxiv.org/abs/2302.01170>.

Köhler, J., Klein, L., and Noé, F. Equivariant flows: Exact likelihood generative learning for symmetric densities. In III, H. D. and Singh, A. (eds.), *Proceedings of the 37th International Conference on Machine Learning*, volume 119 of *Proceedings of Machine Learning Research*, pp. 5361–5370. PMLR, 13–18 Jul 2020. URL <https://proceedings.mlr.press/v119/kohler20a.html>.

Kohler, J., Chen, Y., Kramer, A., Clementi, C., and Noé, F. Flow-matching: Efficient coarse-graining of molecular dynamics without forces. *Journal of Chemical Theory and Computation*, 19(3):942–952, 2023.

Krishna, V., Noid, W. G., and Voth, G. A. The multiscale coarse-graining method. iv. transferring coarse-grained potentials between temperatures. *The Journal of chemical physics*, 131(2), 2009.

Laio, A. and Gervasio, F. L. Metadynamics: a method to simulate rare events and reconstruct the free energy in biophysics, chemistry and material science. *Reports on Progress in Physics*, 71(12):126601, 2008.

Lewis, S., Hempel, T., Jiménez-Luna, J., Gastegger, M., Xie, Y., Foong, A. Y., Satorras, V. G., Abdin, O., Veeling, B. S., Zaporozhets, I., et al. Scalable emulation of protein equilibrium ensembles with generative deep learning. *Science*, pp. eadv9817, 2025.

Lindorff-Larsen, K., Piana, S., Palmo, K., Maragakis, P., Klepeis, J. L., Dror, R. O., and Shaw, D. E. Improved side-chain torsion potentials for the amber ff99sb protein force field. *Proteins: Structure, Function, and Bioinformatics*, 78(8):1950–1958, 2010.

Lindorff-Larsen, K., Piana, S., Dror, R. O., and Shaw, D. E. How fast-folding proteins fold. *Science*, 334(6055):517–520, 2011.

Lipman, Y., Chen, R. T., Ben-Hamu, H., Nickel, M., and Le, M. Flow matching for generative modeling. *arXiv preprint arXiv:2210.02747*, 2022.

Liu, G.-H., Choi, J., Chen, Y., Miller, B. K., and Chen, R. T. Adjoint schrödinger bridge sampler. *arXiv preprint arXiv:2506.22565*, 2025.

Liu, X., Gong, C., and Liu, Q. Flow straight and fast: Learning to generate and transfer data with rectified flow, 2022. URL <https://arxiv.org/abs/2209.03003>.

Majewski, M., Pérez, A., Thölke, P., Doerr, S., Charron, N. E., Giorgino, T., Husic, B. E., Clementi, C., Noé, F., and De Fabritiis, G. Machine learning coarse-grained potentials of protein thermodynamics. *Nature Communications*, 14(1), September 2023. ISSN 2041-1723. doi: 10.1038/s41467-023-41343-1. URL <http://dx.doi.org/10.1038/s41467-023-41343-1>.

Marrink, S. J., Risselada, H. J., Yefimov, S., Tieleman, D. P., and de Vries, A. H. The MARTINI Force Field: Coarse Grained Model for Biomolecular Simulations. *The Journal of Physical Chemistry B*, 111(27):7812–7824, July 2007. ISSN 1520-6106. doi: 10.1021/jp071097f.

Mehdi, S., Smith, Z., Herron, L., Zou, Z., and Tiwary, P. Enhanced sampling with machine learning. *Annual Review of Physical Chemistry*, 75(2024):347–370, 2024.

Midgley, L. I., Stumper, V., Simm, G. N. C., Schölkopf, B., and Hernández-Lobato, J. M. Flow annealed importance sampling bootstrap, 2023. URL <https://arxiv.org/abs/2208.01893>.

Mirarchi, A., Peláez, R. P., Simeon, G., and De Fabritiis, G. Amaro: All heavy-atom transferable neural network potentials of protein thermodynamics. *Journal of Chemical Theory and Computation*, 20(22):9871–9878, 2024.

Moqvist, S., Chen, W., Schreiner, M., N’uske, F., and Olsson, S. Thermodynamic interpolation: A generative approach to molecular thermodynamics and kinetics. *Journal of Chemical Theory and Computation*, 21(5):2535–2545, 2025.

Musil, F., Willatt, M. J., Langovoy, M. A., and Ceriotti, M. Fast and accurate uncertainty estimation in chemical machine learning. *Journal of chemical theory and computation*, 15(2):906–915, 2019.

Nam, J., Máté, B., Toshev, A. P., Kaniselvan, M., Gómez-Bombarelli, R., Chen, R. T., Wood, B., Liu, G.-H., and Miller, B. K. Enhancing diffusion-based sampling with molecular collective variables. *arXiv preprint arXiv:2510.11923*, 2025.

Nguyen, H., Roe, D. R., and Simmerling, C. Improved generalized born solvent model parameters for protein simulations. *Journal of chemical theory and computation*, 9(4):2020–2034, 2013.

Noid, W. G. Perspective: Coarse-grained models for biomolecular systems. *The Journal of Chemical Physics*, 139(9):090901, September 2013. ISSN 0021-9606. doi: 10.1063/1.4818908.

Noid, W. G., Chu, J.-W., Ayton, G. S., Krishna, V., Izvekov, S., Voth, G. A., Das, A., and Andersen, H. C. The multiscale coarse-graining method. i. a rigorous bridge between atomistic and coarse-grained models. *The Journal of Chemical Physics*, 128(24), June 2008. ISSN 1089-7690. doi: 10.1063/1.2938860. URL <http://dx.doi.org/10.1063/1.2938860>.

Noé, F., Olsson, S., Köhler, J., and Wu, H. Boltzmann generators: Sampling equilibrium states of many-body systems with deep learning. *Science*, 365(6457), September 2019. ISSN 1095-9203. doi: 10.1126/science.aaw1147. URL <http://dx.doi.org/10.1126/science.aaw1147>.

Olsson, S. Generative molecular dynamics. *Current Opinion in Structural Biology*, 96:103213, 2026.

Onufriev, A., Bashford, D., and Case, D. A. Exploring protein native states and large-scale conformational changes with a modified generalized born model. *Proteins: Structure, Function, and Bioinformatics*, 55(2):383–394, 2004.

Peng, X. and Gao, A. Flow perturbation to accelerate boltzmann sampling. *Nature Communications*, 16(1):6604, 2025.

Plainer, M., Wu, H., Klein, L., Günemann, S., and Noé, F. Consistent sampling and simulation: Molecular dynamics with energy-based diffusion models. *arXiv preprint arXiv:2506.17139*, 2025.

Potapchik, P., Lee, C.-K., and Albergo, M. S. Tilt matching for scalable sampling and fine-tuning. *arXiv preprint arXiv:2512.21829*, 2025.

Raja, S., Šípká, M., Psenka, M., Kreiman, T., Pavelka, M., and Krishnapriyan, A. S. Action-minimization meets generative modeling: Efficient transition path sampling with the onsager-machlup functional. *arXiv preprint arXiv:2504.18506*, 2025.

Ramachandran, G. N. Stereochemistry of polypeptide chain configurations. *J. Mol. Biol.*, 7:95–99, 1963.

Rehman, D., Akhound-Sadegh, T., Gazizov, A., Bengio, Y., and Tong, A. Falcon: Few-step accurate likelihoods for continuous flows. *arXiv preprint arXiv:2512.09914*, 2025.

Rezende, D. J. and Mohamed, S. Variational inference with normalizing flows, 2016.

Ribeiro, J. M. L., Bravo, P., Wang, Y., and Tiwary, P. Reweighted autoencoded variational bayes for enhanced sampling (rave). *The Journal of chemical physics*, 149(7), 2018.

Rotskoff, G. M. Sampling thermodynamic ensembles of molecular systems with generative neural networks: Will integrating physics-based models close the generalization gap? *Current Opinion in Solid State and Materials Science*, 30:101158, 2024.

Saunders, M. G. and Voth, G. A. Coarse-graining methods for computational biology. *Annual review of biophysics*, 42(1):73–93, 2013.

Schebek, M. and Rogal, J. Scalable boltzmann generators for equilibrium sampling of large-scale materials. *arXiv preprint arXiv:2509.25486*, 2025.

Schoenholz, S. and Cubuk, E. D. Jax md: a framework for differentiable physics. *Advances in Neural Information Processing Systems*, 33:11428–11441, 2020.

Schopmans, H. and Friederich, P. Conditional normalizing flows for active learning of coarse-grained molecular representations. In *International Conference on Machine Learning*, pp. 43804–43827. PMLR, 2024.

Schreiner, M., Winther, O., and Olsson, S. Implicit transfer operator learning: Multiple time-resolution models for molecular dynamics. *Advances in Neural Information Processing Systems*, 36:36449–36462, 2023.

Shell, M. S. The relative entropy is fundamental to multi-scale and inverse thermodynamic problems. *The Journal of chemical physics*, 129(14), 2008.

Shi, Y., Huang, Z., Feng, S., Zhong, H., Wang, W., and Sun, Y. Masked label prediction: Unified message passing model for semi-supervised classification. *arXiv preprint arXiv:2009.03509*, 2020.

Souza, P. C., Alessandri, R., Barnoud, J., Thallmair, S., Faustino, I., Grünewald, F., Patmanidis, I., Abdizadeh, H., Bruininks, B. M., Wassenaar, T. A., et al. Martini 3: a general purpose force field for coarse-grained molecular dynamics. *Nature methods*, 18(4):382–388, 2021.

Stukowski, A. Visualization and analysis of atomistic simulation data with ovlito—the open visualization tool. *Modelling and simulation in materials science and engineering*, 18(1):015012, 2009.

Stupp, M. and Koutsourelakis, P. Energy-based coarse-graining in molecular dynamics: A flow-based framework without data. *arXiv preprint arXiv:2504.20940*, 2025.

Tamagnone, S., Laio, A., and Gabrié, M. Coarse-grained molecular dynamics with normalizing flows. *Journal of Chemical Theory and Computation*, 20(18):7796–7805, 2024.

Tan, C. B., Bose, A. J., Lin, C., Klein, L., Bronstein, M. M., and Tong, A. Scalable equilibrium sampling with sequential boltzmann generators. *arXiv preprint arXiv:2502.18462*, 2025a.

Tan, C. B., Hassan, M., Klein, L., Syed, S., Beaini, D., Bronstein, M. M., Tong, A., and Neklyudov, K. Amortized sampling with transferable normalizing flows. *arXiv preprint arXiv:2508.18175*, 2025b.

Thaler, S. and Zavadlav, J. Learning neural network potentials from experimental data via differentiable trajectory reweighting. *Nature communications*, 12(1):6884, 2021.

Thaler, S., Stupp, M., and Zavadlav, J. Deep coarse-grained potentials via relative entropy minimization. *The Journal of Chemical Physics*, 157(24):244103, December 2022. ISSN 0021-9606. doi: 10.1063/5.0124538.

Tong, A., Fatras, K., Malkin, N., Huguet, G., Zhang, Y., Rector-Brooks, J., Wolf, G., and Bengio, Y. Improving and generalizing flow-based generative models with mini-batch optimal transport. *arXiv preprint arXiv:2302.00482*, 2023.

Torrie, G. and Valleau, J. Nonphysical sampling distributions in monte carlo free-energy estimation: Umbrella sampling. *Journal of Computational Physics*, 23(2):187–199, February 1977. doi: 10.1016/0021-9991(77)90121-8. URL [https://doi.org/10.1016/0021-9991\(77\)90121-8](https://doi.org/10.1016/0021-9991(77)90121-8).

Unke, O. T., Chmiela, S., Sauceda, H. E., Gastegger, M., Poltavsky, I., Schutt, K. T., Tkatchenko, A., and Muller, K.-R. Machine learning force fields. *Chemical Reviews*, 121(16):10142–10186, 2021.

Van Der Spoel, D., Lindahl, E., Hess, B., Groenhof, G., Mark, A. E., and Berendsen, H. J. Gromacs: fast, flexible, and free. *Journal of computational chemistry*, 26(16):1701–1718, 2005.

Vempala, S. and Wibisono, A. Rapid convergence of the unadjusted langevin algorithm: Isoperimetry suffices. *Advances in neural information processing systems*, 32, 2019.

Vlachas, P. R., Zavadlav, J., Praprotnik, M., and Koumoutsakos, P. Accelerated simulations of molecular systems through learning of effective dynamics. *Journal of Chemical Theory and Computation*, 18(1):538–549, 2021.

von Klitzing, C., Blessing, D., Schopmans, H., Friederich, P., and Neumann, G. Learning boltzmann generators via constrained mass transport. *arXiv preprint arXiv:2510.18460*, 2025.

Wang, J., Olsson, S., Wehmeyer, C., Pérez, A., Charron, N. E., de Fabritiis, G., Noé, F., and Clementi, C. Machine learning of coarse-grained molecular dynamics force fields. *ACS Central Science*, 5(5):755–767, April 2019. ISSN 2374-7951. doi: 10.1021/acscentsci.8b00913. URL <http://dx.doi.org/10.1021/acscentsci.8b00913>.

Wang, W., Xu, M., Cai, C., Miller, B. K., Smidt, T., Wang, Y., Tang, J., and Gómez-Bombarelli, R. Generative coarse-graining of molecular conformations. *arXiv preprint arXiv:2201.12176*, 2022.

Wirnsberger, P., Ballard, A. J., Papamakarios, G., Abercrombie, S., Racanière, S., Pritzel, A., Jimenez Rezende, D., and Blundell, C. Targeted free energy estimation via learned mappings. *The Journal of Chemical Physics*, 153(14), October 2020. ISSN 1089-7690. doi: 10.1063/5.0018903. URL <http://dx.doi.org/10.1063/5.0018903>.

Wood, B. M., Dzamba, M., Fu, X., Gao, M., Shuaibi, M., Barroso-Luque, L., Abdelmaqsoud, K., Gharakhanyan, V., Kitchin, J. R., Levine, D. S., et al. Uma: A family of universal models for atoms. *arXiv preprint arXiv:2506.23971*, 2025.

Xu, Y., Wang, D., Zhou, Z., Yu, T., and Chen, M. Tempo: Temporal multi-scale autoregressive generation of protein conformational ensembles. *arXiv preprint arXiv:2511.05510*, 2025.

Zaverkin, V., Holzmüller, D., Christiansen, H., Errica, F., Alesiani, F., Takamoto, M., Niepert, M., and Kästner, J. Uncertainty-biased molecular dynamics for learning uniformly accurate interatomic potentials. *npj Computational Materials*, 10(1):83, 2024.

Zhai, S., Zhang, R., Nakkiran, P., Berthelot, D., Gu, J., Zheng, H., Chen, T., Bautista, M. A., Jaitly, N., and Susskind, J. Normalizing flows are capable generative models. *arXiv preprint arXiv:2412.06329*, 2024.

Zhang, L., Han, J., Wang, H., Car, R., and E, W. DeePCG: Constructing coarse-grained models via deep neural networks. *The Journal of Chemical Physics*, 149(3): 034101, July 2018. ISSN 0021-9606, 1089-7690. doi: 10.1063/1.5027645.

Zhang, M., Zhang, Z., Wu, H., and Wang, Y. Flow matching for optimal reaction coordinates of biomolecular systems. *Journal of Chemical Theory and Computation*, 21(1): 399–412, 2024.

Zheng, S., He, J., Liu, C., Shi, Y., Lu, Z., Feng, W., Ju, F., Wang, J., Zhu, J., Min, Y., et al. Predicting equilibrium distributions for molecular systems with deep learning. *Nature Machine Intelligence*, 6(5):558–567, 2024.

Zhu, J., Bülow, S. v., Liu, H., Lindorff-Larsen, K., and Chen, H. Extending conformational ensemble prediction to multidomain proteins and protein complex. *bioRxiv*, pp. 2026–01, 2026.

Zhu, K., Trizio, E., Zhang, J., Hu, R., Jiang, L., Hou, T., and Bonati, L. Enhanced sampling in the age of machine learning: Algorithms and applications. *Chemical Reviews*, 2025.

A. Proofs

A.1. Proof of Proposition 1

Proposition 1. Let $p^*(\mathbf{R}) \propto e^{-\beta U^*(\mathbf{R})}$ be the true marginal and $p_\eta(\mathbf{R}) \propto e^{-\beta U_\eta(\mathbf{R})}$ the learned distribution. If p^* satisfies a Logarithmic Sobolev Inequality (LSI) with constant $\rho > 0$. Then, the Kullback-Leibler divergence between the learned and true distributions is bounded by the expected squared force error:

$$\mathcal{D}_{\text{KL}}(p_\eta \| p^*) \leq \frac{\beta^2}{2\rho} \mathbb{E}_{p_\eta} [\|\nabla U_\eta(\mathbf{R}) - \nabla U^*(\mathbf{R})\|^2]. \quad (14)$$

Proof. The Kullback-Leibler divergence is defined as:

$$\mathcal{D}_{\text{KL}}(p_\eta \| p^*) = \int p_\eta(\mathbf{R}) \log \frac{p_\eta(\mathbf{R})}{p^*(\mathbf{R})} d\mathbf{R}. \quad (19)$$

The Fisher Divergence (or relative Fisher information) between p_η and p^* is defined as:

$$\mathcal{J}(p_\eta \| p^*) = \int p_\eta(\mathbf{R}) \|\nabla \log p_\eta(\mathbf{R}) - \nabla \log p^*(\mathbf{R})\|^2 d\mathbf{R}. \quad (20)$$

Since $p_\eta(\mathbf{R}) = Z_\eta^{-1} e^{-\beta U_\eta(\mathbf{R})}$ and $p^*(\mathbf{R}) = (Z^*)^{-1} e^{-\beta U^*(\mathbf{R})}$, the gradients of the log-densities are directly proportional to the forces:

$$\nabla \log p_\eta(\mathbf{R}) = -\beta \nabla U_\eta(\mathbf{R}), \quad \nabla \log p^*(\mathbf{R}) = -\beta \nabla U^*(\mathbf{R}). \quad (21)$$

Substituting these into the definition of the Fisher Divergence:

$$\mathcal{J}(p_\eta \| p^*) = \int p_\eta(\mathbf{R}) \|(-\beta \nabla U_\eta(\mathbf{R})) - (-\beta \nabla U^*(\mathbf{R}))\|^2 d\mathbf{R} \quad (22)$$

$$= \beta^2 \int p_\eta(\mathbf{R}) \|\nabla U_\eta(\mathbf{R}) - \nabla U^*(\mathbf{R})\|^2 d\mathbf{R} \quad (23)$$

$$= \beta^2 \mathbb{E}_{p_\eta} [\|\mathcal{F}_\eta(\mathbf{R}) - \mathcal{F}^*(\mathbf{R})\|^2]. \quad (24)$$

We assume that the target distribution p^* satisfies a Logarithmic Sobolev Inequality (LSI) with constant $\rho > 0$. By definition, this inequality implies that for any distribution p_η absolutely continuous with respect to p^* :

$$\mathcal{D}_{\text{KL}}(p_\eta \| p^*) \leq \frac{1}{2\rho} \mathcal{J}(p_\eta \| p^*). \quad (25)$$

Substituting our expression for the Fisher Divergence into the LSI yields the final bound:

$$\mathcal{D}_{\text{KL}}(p_\eta \| p^*) \leq \frac{1}{2\rho} (\beta^2 \mathbb{E}_{p_\eta} [\|\nabla U_\eta(\mathbf{R}) - \nabla U^*(\mathbf{R})\|^2]). \quad (26)$$

Dividing out the constants concludes the proof. \square

A.2. Proof of Proposition 2

Proposition 2. (Chen et al. (2026)) Let $V(\mathbf{R})$ be a bias potential depending only on the coarse-grained coordinates. The conditional distribution of atomistic configurations given \mathbf{R} remains unchanged:

$$p_V(\mathbf{r} | \mathbf{R}) = p(\mathbf{r} | \mathbf{R}). \quad (15)$$

Proof. Let $p(\mathbf{r}) = Z^{-1} e^{-\beta u(\mathbf{r})}$ be the unbiased equilibrium distribution. By definition, the unbiased marginal distribution is

$$p(\mathbf{R}) = \int p(\mathbf{r}) \delta(\Xi(\mathbf{r}) - \mathbf{R}) d\mathbf{r} = \frac{1}{Z} \int e^{-\beta u(\mathbf{r})} \delta(\Xi(\mathbf{r}) - \mathbf{R}) d\mathbf{r}. \quad (27)$$

Rearranging this yields the identity for the unnormalized marginal:

$$\int e^{-\beta u(\mathbf{r})} \delta(\Xi(\mathbf{r}) - \mathbf{R}) d\mathbf{r} = Zp(\mathbf{R}). \quad (28)$$

Now, consider the biased distribution $p_V(\mathbf{r}) = Z_V^{-1} e^{-\beta(u(\mathbf{r}) + V(\Xi(\mathbf{r})))}$. The biased marginal distribution is:

$$p_V(\mathbf{R}) = \int \frac{e^{-\beta u(\mathbf{r})} e^{-\beta V(\Xi(\mathbf{r}))}}{Z_V} \delta(\Xi(\mathbf{r}) - \mathbf{R}) d\mathbf{r} \quad (29)$$

$$= \frac{e^{-\beta V(\mathbf{R})}}{Z_V} \underbrace{\int e^{-\beta u(\mathbf{r})} \delta(\Xi(\mathbf{r}) - \mathbf{R}) d\mathbf{r}}_{=Zp(\mathbf{R}) \text{ (from Eq. 28)}} \quad (30)$$

$$= \frac{Z}{Z_V} e^{-\beta V(\mathbf{R})} p(\mathbf{R}). \quad (31)$$

Finally, substituting this into the definition of the conditional distribution:

$$p_V(\mathbf{r} | \mathbf{R}) = \frac{p_V(\mathbf{r}) \delta(\Xi(\mathbf{r}) - \mathbf{R})}{p_V(\mathbf{R})} = \frac{Z_V^{-1} e^{-\beta u(\mathbf{r})} e^{-\beta V(\mathbf{R})} \delta(\dots)}{\frac{Z}{Z_V} e^{-\beta V(\mathbf{R})} p(\mathbf{R})} = \frac{e^{-\beta u(\mathbf{r})} \delta(\dots)}{Zp(\mathbf{R})} = p(\mathbf{r} | \mathbf{R}). \quad (32)$$

□

B. Datasets

B.1. Müller-Brown Potential

Potential Parameters. For the two-dimensional toy system, we use a Müller–Brown potential defined as

$$u(x, y) = u_1(x, y) + u_2(x, y) + u_3(x, y) + u_4(x, y), \quad (33)$$

with (Raja et al., 2025)

$$\begin{aligned} u_1(x, y) &= -17.3 \exp \left[-0.0039(x - 48)^2 - 0.0391(y - 8)^2 \right], \\ u_2(x, y) &= -8.7 \exp \left[-0.0039(x - 32)^2 - 0.0391(y - 16)^2 \right], \\ u_3(x, y) &= -14.7 \exp \left[-0.0254(x - 24)^2 + 0.043(x - 24)(y - 32) - 0.0254(y - 32)^2 \right], \\ u_4(x, y) &= 1.3 \exp \left[0.00273(x - 16)^2 + 0.0023(x - 16)(y - 24) + 0.00273(y - 24)^2 \right]. \end{aligned}$$

Umbrella Sampling. For umbrella sampling, we introduce a biasing potential along the x coordinate,

$$V_x(x) = -4 \exp \left[-\frac{(x - 32.0)^2}{2 \cdot 5^2} \right].$$

This enables better sampling of the configurations around $\mathbf{x}_0 = 32$, allowing a better representation of transition regions that are otherwise rarely visited in unbiased trajectories.

Simulation Details. For the MB dataset generation, we perform two-dimensional Langevin dynamics with a time step of 0.1, mass $m = 1.0$, friction coefficient $\gamma = 0.1$, and temperature $k_B T = 1.0$. Ten independent trajectories of length 10^7 steps are generated, with initial positions sampled uniformly from $[10, 50]^2$ and initial velocities drawn from a Gaussian distribution with standard deviation 0.1. Configurations are recorded every 10 steps. The dynamics follow

$$m\ddot{\mathbf{r}} = -\nabla(u(\mathbf{r}) + V(x)) - \gamma m\dot{\mathbf{r}} + \sqrt{2\gamma k_B T m} \boldsymbol{\eta}(t), \quad (34)$$

where $V(x)$ is the applied bias, and $\boldsymbol{\eta}(t)$ denotes Gaussian white noise. For each saved configuration, unbiased forces from ∇u are computed and stored.

B.2. Alanine Dipeptide

Force Fields. For the explicit solvent dataset, alanine dipeptide is parameterized using the AMBER99SB-ILDN force field (Lindorff-Larsen et al., 2010) and solvated in a cubic box of TIP3P water molecules. All explicit solvent simulations are carried out with GROMACS (Van Der Spoel et al., 2005). For the implicit solvent dataset, the same force field is used together with the generalized Born (OBC1/OBC2) implicit solvent model, and simulations are performed using OpenMM (Eastman et al., 2023).

Well-Tempered Metadynamics. We perform well-tempered metadynamics (WT-MetaD) (Barducci et al., 2008) simulations of alanine dipeptide in explicit solvent using GROMACS coupled with PLUMED (Bonomi et al., 2009). The backbone dihedral angles ϕ (C–N–C α –C) and ψ (N–C α –C–N) are chosen as collective variables. Gaussian hills with height 1.2 kJ/mol and width 0.35 rad are deposited every 500 integration steps (1 ps). Datasets are generated with bias factors $\gamma = 1.5$ and $\gamma = 9$, where $\gamma = 1.5$ is used to train flow model for biased proposal generation and $\gamma = 9$ is used for enhanced sampling force matching. Each simulation is run for 2×10^7 steps (10 ns) with a time step of 0.5 fs and no bond constraints. Positions and forces are recorded every 40 steps (0.02 ps), yielding 5×10^5 saved configurations per dataset. To ensure unbiased force labels, all forces are recomputed by rerunning the saved trajectories in GROMACS without the metadynamics bias using the `mdrun -rerun` functionality. This guarantees that each configuration is associated with forces from the underlying unbiased potential.

Simulation Details. All simulations are performed in the NVT ensemble at a temperature of 300 K. For explicit solvent systems, alanine dipeptide is solvated in a cubic box of TIP3P water with a side length of 3.7 nm. After energy minimization, production dynamics are carried out using a velocity-rescale thermostat (time constant 0.1 ps). Long-range electrostatics are treated using the particle mesh Ewald method, and van der Waals interactions are truncated at 1.0 nm. We summarize the dataset configurations used in this work in Tab. 3.

Table 3. Overview of simulation details for alanine dipeptide datasets.

Solvent	Dataset	Method	Length	Timestep	Constraints
Explicit (TIP3P)	Unbiased MD	None	500 ns	0.5 fs	None
Explicit (TIP3P)	Biased MD (for CNF)	WT-MetaD ($\gamma = 1.5$)	10 ns	0.5 fs	None
Explicit (TIP3P)	Biased MD (for PMF)	WT-MetaD ($\gamma = 9$)	10 ns	0.5 fs	None
Implicit (OBC1)	Unbiased MD	None	500 ns	2 fs	H-bonds
Implicit (OBC2)	Unbiased MD	None	500 ns	2 fs	H-bonds

C. Experimental Details for Conditional Normalizing Flows

C.1. Architecture

Müller-Brown Potential. For MB potential, we use a multilayer perceptron augmented with time conditioning for flow matching. The network consists of three hidden layers with width 96. Flow time is embedded into a 16-dimensional time embedding and concatenated with the input.

Alanine Dipeptide. For the alanine dipeptide, we use an adapted Graph Transformer architecture (Plainer et al., 2025; Arts et al., 2023; Shi et al., 2020). Given bead positions \mathbf{x}_i and bead features \mathbf{h}_i , edge attributes are constructed as

$$\mathbf{d}_{ij} = \mathbf{x}_i - \mathbf{x}_j, \quad r_{ij} = \|\mathbf{d}_{ij}\|, \quad \mathbf{e}_{ij} = [\mathbf{d}_{ij}, r_{ij}], \quad (35)$$

and node attributes are initialized as

$$\mathbf{n}_i^{(0)} = [\mathbf{h}_i, \mathbf{x}_i, t], \quad (36)$$

where t denotes the flow time. The bead features and time are embedded into 16- and 4-dimensional vectors, respectively, concatenated with positions, and projected to 128-dimensional node embeddings via a linear layer. Edge attributes are also embedded into 128 dimensions. The model consists of three Graph Transformer layers with 8 attention heads and a head dimension of 64. To enforce rotational equivariance, random global rotations are applied to molecular configurations during training as data augmentation (Abramson et al., 2024).

C.2. Training Configuration

For alanine dipeptide, models are trained using AdamW with weight decay 10^{-5} and a cosine learning-rate schedule ranging from 3×10^{-4} to 1×10^{-5} , using a batch size of 256 for 5000 epochs. For MB potential, we use the same configuration except training for 2000 epochs. We find no consistent benefit from exponential moving average (EMA) of parameters and therefore do not use it in our experiments.

C.3. Inference

As Hutchinson’s trace estimator introduces bias for BGs (Tan et al., 2025a; Peng & Gao, 2025), we compute the divergence exactly using automatic differentiation. For inference, we use the Dormand–Prince 5(4) method (`dopr5`) with absolute and relative tolerances set to 10^{-4} . Inference is performed with a batch size of 1000.

C.4. Computational Cost

The reported inference times (Tab. 4) correspond to generating 10^4 samples. All other training and inference parameters are provided in §C.2 and §C.3. A batch size of 1000 is used for all experiments, except for the all-atom mapping, which uses a batch size of 512 due to GPU memory constraints.

Table 4. Training and inference time for CFM across settings. Inference times correspond to 10^4 generated samples. Results marked with \dagger are from (Rehman et al., 2025).

	Core Beta	Heavy Atom	All Atom	ECNF++ \dagger	SBG \dagger	DiT CNF \dagger	FALCON \dagger
Training	0.83h	1.39h	3.93h	–	–	–	–
Inference	0.84min	3.46min	13.92min	–	–	–	–
Total	0.84h	1.45h	4.16h	12.52h	16.83h	9.56h	7.65h

D. Experimental Details for Force Matching

D.1. Architecture

Müller-Brown Potential. For the MB potential, we use a radial basis function (RBF) feature map followed by a multilayer perceptron. The RBF expansion has $K = 100$ centers, initialized uniformly in $[10, 50]^2$ and optimized during training, with a fixed width $\sigma = 5.0$. The features are passed through four fully connected layers of size 128 with softplus activation, followed by a linear output layer.

Alanine Dipeptide. For alanine dipeptide, the CG potential $U_\eta(\mathbf{R})$ is parameterized using the MACE architecture (Batatia et al., 2022), an equivariant message-passing graph neural network. Each CG bead is represented as a node in a geometric graph, with edges connecting neighbors within a cutoff radius and encoding relative position vectors. The model uses hidden irreducible representations of $32 \times 0e + 32 \times 1o$, processed through two interaction layers with correlation order 3 and an angular momentum expansion truncated at $\ell_{\max} = 3$. Node features are decoded by a readout layer ($16 \times 0e$) into a scalar energy prediction ($1 \times 0e$). Periodic displacement functions are applied during graph construction to handle boundary conditions correctly.

D.2. Training Configuration

For MB, training uses the Adam optimizer (via Optax) with a constant learning rate of 10^{-4} and batch size 128 for 500 epochs. For alanine dipeptide, training uses Adam with exponential learning rate decay ($\eta_0 = 10^{-3}$, decay rate 0.9), batch size 256, and 250 epochs. Training and validation splits are with a 90/10 ratio. Gradients are clipped to a global norm of 1.0. The final parameters for energy evaluation correspond to the minimum validation loss.

D.3. Computational Cost

The reported inference times (Tab. 5) correspond to evaluating 10^4 samples. Training parameters follow §D.2. A batch size of 500 is used for inference.

Table 5. Training and inference time for MACE model. Inference times correspond to 10^4 samples evaluated.

	Core Beta	Heavy Atom
Training	1.88h	4.11h
Inference	0.66s	0.72s

E. Compute Infrastructure and Software

E.1. Hardware

All experiments, including model training, inference, and computational benchmarks, are performed on a single NVIDIA A100 GPU with 80 GB memory.

E.2. Software

CFM is implemented using JAX, DiffraX (Kidger, 2021), and Flax (Heek et al., 2024). Graph transformer is adapted from the implementation provided in https://github.com/noegroup/ScoreMD/blob/main/src/scoremd/models/graph_transformer.py. Training of CG PMF is carried out using chemtrain (Fuchs et al., 2025b) and chemtrain-deploy (Fuchs et al., 2025a) built on JAX, M.D. (Schoenholz & Cubuk, 2020). Molecular structures are visualized using OVITO (Stukowski, 2009).

F. Algorithms

Algorithm 1 Training CG PMF via ESFM

Input: Dataset $\mathcal{D}_{\text{bias}} = \{(\mathbf{r}, \mathcal{F}_{\text{proj}}(\mathbf{r}))\}$ (Rapidly converged); batch size B
Initialize: CG PMF network U_η
while not converged **do**
 Sample $\{(\mathbf{r}^{(i)}, \mathcal{F}_{\text{proj}}^{(i)})\}_{i=1}^B \sim \mathcal{D}_{\text{bias}}$
 Compute $\mathbf{R}^{(i)} \leftarrow \Xi(\mathbf{r}^{(i)})$
 $\mathcal{L}_{\text{ESFM}} \leftarrow \frac{1}{B} \sum_{i=1}^B \|\nabla_{\mathbf{R}} U_\eta(\mathbf{R}^{(i)}) - \mathcal{F}_{\text{proj}}^{(i)}\|_2^2$
 Update $\eta \leftarrow \text{Optim}(\eta, \nabla_\eta \mathcal{L}_{\text{ESFM}})$
end while
Return U_η

Algorithm 2 Training Flow Model via CFM

Input: Dataset $\mathcal{D} = \{\mathbf{r}\}$ (biased or unbiased); batch size B
Initialize: flow model v_θ
while not converged **do**
 Sample $\mathbf{r}^{(i)} \sim \mathcal{D}$
 Compute $\mathbf{R}_1^{(i)} \leftarrow \Xi(\mathbf{r}^{(i)})$
 Sample $\mathbf{R}_0^{(i)} \sim \mathcal{N}(\mathbf{0}, \mathbf{I})$
 Sample $t^{(i)} \sim \mathcal{U}[0, 1]$
 $\mathbf{R}_t^{(i)} \leftarrow (1 - t^{(i)})\mathbf{R}_0^{(i)} + t^{(i)}\mathbf{R}_1^{(i)}$
 $u_t^{(i)} \leftarrow \mathbf{R}_1^{(i)} - \mathbf{R}_0^{(i)}$
 $\mathcal{L}_{\text{CFM}} \leftarrow \frac{1}{B} \sum_{i=1}^B \|v_\theta(t^{(i)}, \mathbf{R}_t^{(i)}) - u_t^{(i)}\|_2^2$
 Update $\theta \leftarrow \text{Optim}(\theta, \nabla_\theta \mathcal{L}_{\text{CFM}})$
end while
Return v_θ

Algorithm 3 Sampling & Reweighting

Input: Trained models U_η, v_θ ; number of samples N
 Initialize sample set $\mathcal{X} \leftarrow \emptyset$, log-weights $\mathcal{W} \leftarrow \emptyset$
for $i = 1$ to N **do**
 Sample $\mathbf{z} \sim \mathcal{N}(\mathbf{0}, \mathbf{I})$
 Solve ODE $\frac{d\mathbf{R}}{dt} = v_\theta(t, \mathbf{R})$ with $\mathbf{R}(0) = \mathbf{z}$
 $\mathbf{R}^{(i)} \leftarrow \mathbf{R}(1)$
 $\Delta\ell^{(i)} \leftarrow \int_0^1 \nabla \cdot v_\theta(t, \mathbf{R}(t)) dt$
 $\log q_\theta(\mathbf{R}^{(i)}) \leftarrow \log p_0(\mathbf{z}) - \Delta\ell^{(i)}$
 $E^{(i)} \leftarrow U_\eta(\mathbf{R}^{(i)})$
 $\log \tilde{w}^{(i)} \leftarrow -\beta E^{(i)} - \log q_\theta(\mathbf{R}^{(i)})$
 Append $\mathbf{R}^{(i)}$ to \mathcal{X} and $\log \tilde{w}^{(i)}$ to \mathcal{W}
end for
 Weight clipping for \mathcal{W}
 Normalize weights $\{w^{(i)}\}$ and compute ESS
Return samples \mathcal{X} , weights $\{w^{(i)}\}$, ESS

G. Additional Results

G.1. Ramachandran Plots

We show Ramachandran plots for alanine dipeptide to illustrate the effect of importance reweighting. Fig. 6 shows the reference distributions from MD simulations in explicit and implicit solvent. Fig. 6b corresponds to a short 10 ns unbiased trajectory, which fails to sample the correct ϕ mode, highlighting the need for enhanced sampling to achieve sufficient configurational coverage.

We compare the MD reference with CG-BG flow proposals before and after reweighting for both mappings (Fig. 7, Fig. 8, Fig. 10, and Fig. 11). Unreweighted proposals exhibit noisy sampling and populate low-probability regions of the free energy landscape. These configurations receive low importance weights and contribute negligibly after reweighting, yielding distributions consistent with the reference.

We further examine reweighted samples obtained using different PMFs. The PMF trained on long unbiased data (PMF_U) underestimates the correct metastable basin of the ϕ angle (Fig. 9), reflecting the limitations of learning CG PMFs from slowly converging unbiased trajectories.

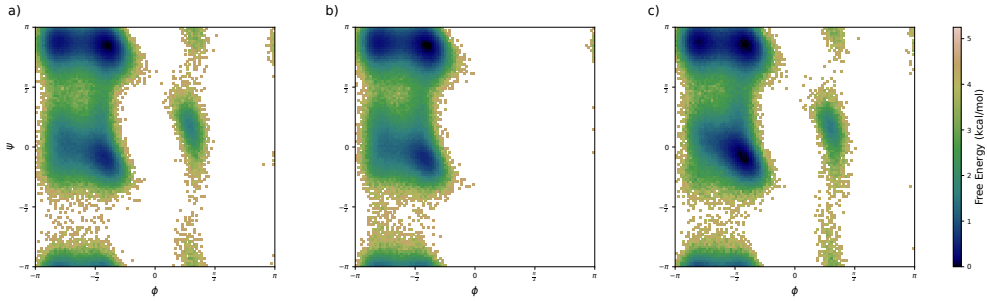


Figure 6. Ramachandran plots for MD simulations. (a) 500 ns unbiased MD simulation (explicit solvent). (b) 10 ns unbiased MD simulation (explicit solvent). (c) 500 ns unbiased MD simulation (implicit solvent) (OBC2).

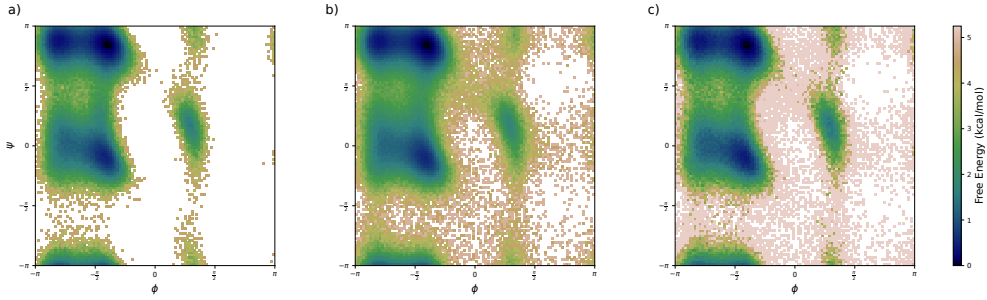


Figure 7. Ramachandran plots (Heavy Atom). (a) MD reference. (b) Flow proposal (flow trained on *unbiased* dataset). (c) Reweighted result (PMF_B).

G.2. Ablation of Weight Clipping

To stabilize importance reweighting, we apply a weight clipping strategy, discarding the top 1% of samples with the largest log-weights.

As shown in Tab. 6, reweighting without clipping leads to large JS divergences and PMF errors, together with near-zero ESS, indicating severe weight degeneracy. In contrast, weight clipping restores stable estimates and substantially improves all metrics.

We further analyze sensitivity to the clipping ratio in Fig. 12. Aggressive clipping (10–20%) maximizes ESS but introduces bias in the reweighted distributions. Small clipping ratios (close to 0%) preserve unbiasedness but suffer from high weights variance. Balancing this bias–variance trade-off, we choose a conservative 1% clipping threshold across all experiments, which yields stable metrics while maintaining physically consistent distributions.

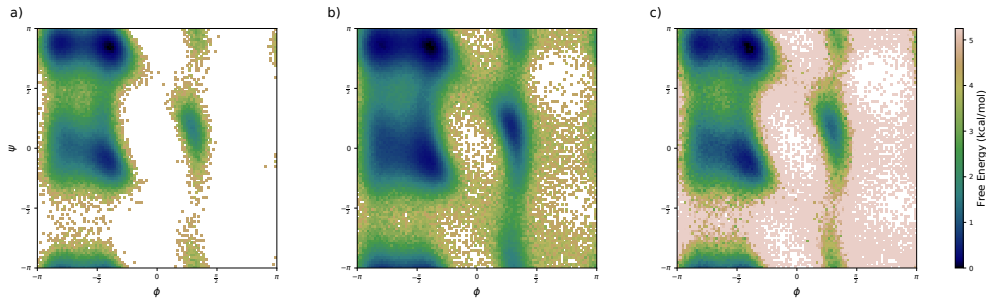


Figure 8. Ramachandran plots (Heavy Atom). (a) MD reference. (b) Flow proposal (flow trained on *WT-MetaD* dataset). (c) Reweighted result (PMF_B).

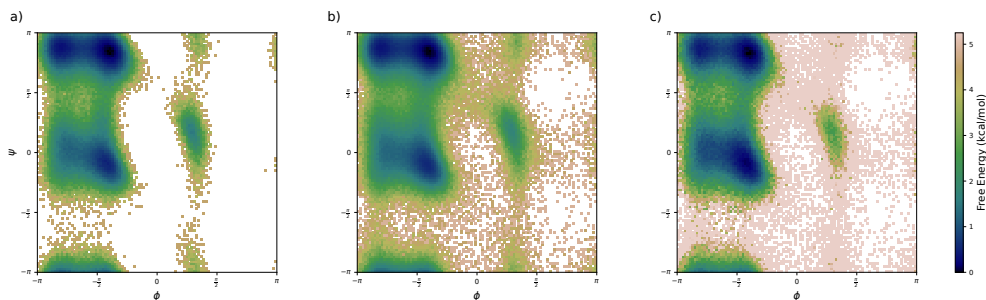


Figure 9. Ramachandran plots (Heavy Atom). (a) MD reference. (b) Flow proposal (flow trained on *unbiased* dataset). (c) Reweighted result (PMF_U).

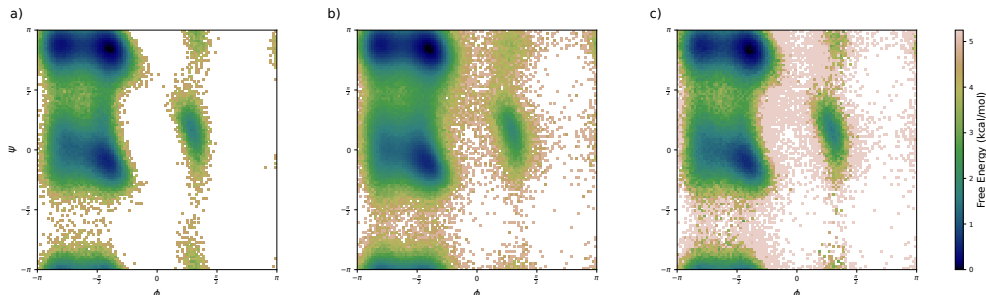


Figure 10. Ramachandran plots (Core Beta). (a) MD reference. (b) Flow proposal (flow trained on *unbiased* dataset). (c) Reweighted result (PMF_B).

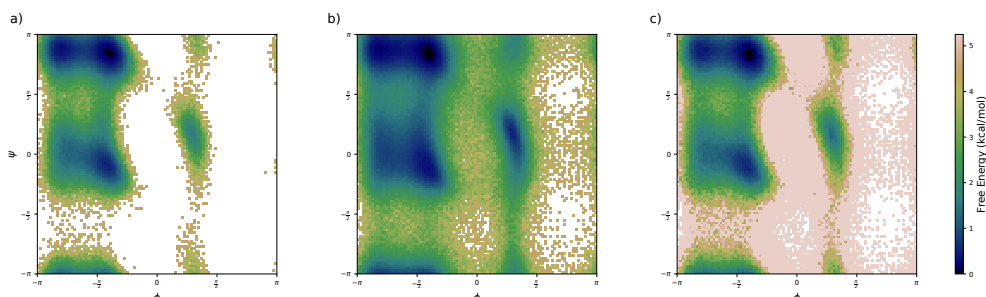


Figure 11. Ramachandran plots (Core Beta). (a) MD reference. (b) Flow proposal (flow trained on *WT-MetaD* dataset). (c) Reweighted result (PMF_B).

Table 6. Quantitative comparison for alanine dipeptide across CG resolutions and different weight clipping thresholds, showing effects on JS, PMF errors, and ESS.

Model	JS (\downarrow)	PMF (\downarrow)	ESS (\uparrow)
Flow Trained on <i>Unbiased</i> Dataset			
Heavy Atom Proposal	0.0074 ± 0.0001	0.6051 ± 0.0102	—
Heavy Atom Reweighted Proposal (1% clip)	0.0075 ± 0.0001	0.2493 ± 0.0126	0.2325 ± 0.0006
Heavy Atom Reweighted Proposal (0% clip)	0.2364 ± 0.0584	8.3338 ± 3.2675	0.0000 ± 0.0001
Core Beta Proposal	0.0072 ± 0.0001	0.5236 ± 0.0099	—
Core Beta Reweighted Proposal (1% clip)	0.0079 ± 0.0001	0.2519 ± 0.0136	0.2510 ± 0.0006
Core Beta Reweighted Proposal (0% clip)	0.2398 ± 0.0923	10.0688 ± 5.6594	0.0001 ± 0.0001
Flow Trained on <i>WT-MetaD</i> Dataset			
Heavy Atom Proposal	0.0505 ± 0.0002	2.5861 ± 0.0353	—
Heavy Atom Reweighted Proposal (1% clip)	0.0090 ± 0.0002	0.2758 ± 0.0109	0.1936 ± 0.0005
Heavy Atom Reweighted Proposal (0% clip)	0.1565 ± 0.0399	6.0221 ± 2.5237	0.0001 ± 0.0001
Core Beta Proposal	0.0540 ± 0.0002	3.7156 ± 0.0393	—
Core Beta Reweighted Proposal (1% clip)	0.0081 ± 0.0001	0.2325 ± 0.0093	0.2239 ± 0.0005
Core Beta Reweighted Proposal (0% clip)	0.5573 ± 0.1692	261.6973 ± 67.6421	N/A

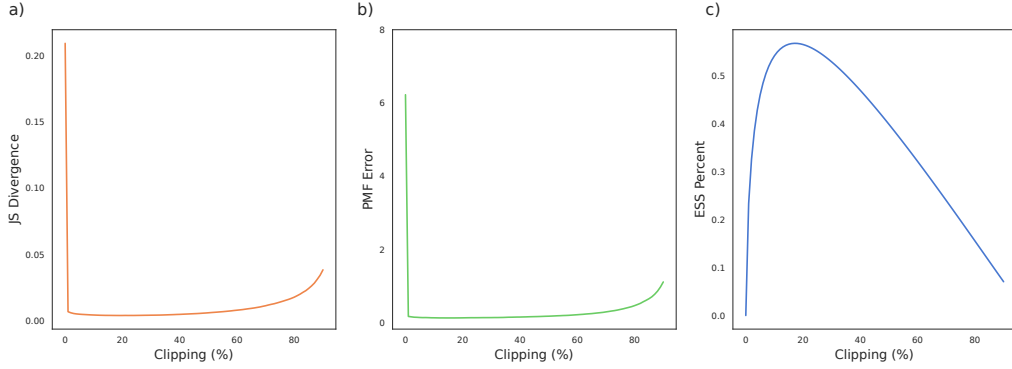


Figure 12. Metrics as a function of weight clipping ratio. (a) JS divergence. (b) PMF error. (c) ESS.

G.3. Free Energy of ψ Dihedral

We provide additional free energy plots for the ψ dihedral of alanine dipeptide (Fig. 13).

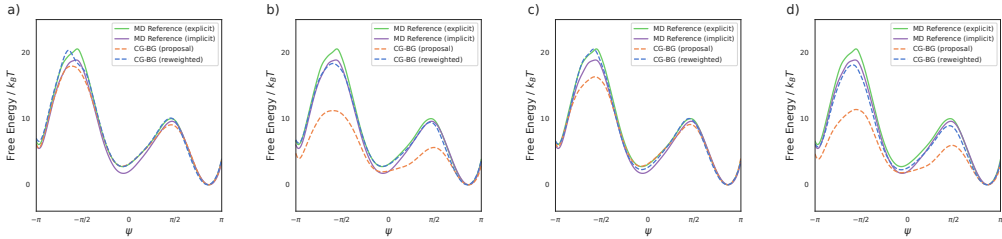


Figure 13. Comparison of ψ dihedral free energy profiles across training settings. All panels show the MD reference alongside CG-BG proposals before and after reweighting. Results correspond to: (a) Flow trained on *unbiased* data (Core Beta); (b) Flow trained on *WT-MetaD* data (Core Beta); (c) Flow trained on *unbiased* (Heavy Atom); (d) Flow trained on *WT-MetaD* data (Heavy Atom).

G.4. Bond Length

Fig. 14 shows the C–N bond length distributions for the MD reference and CG-BG results before and after reweighting.

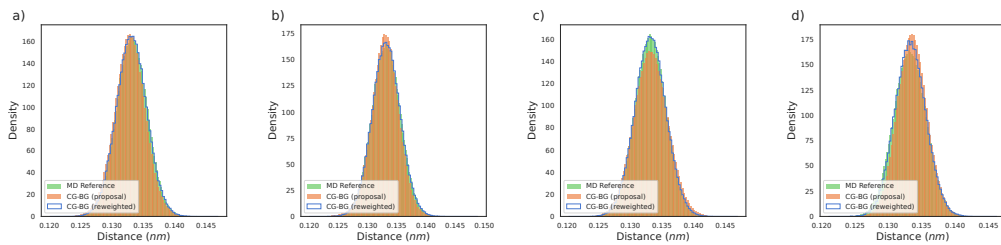


Figure 14. Comparison of C–N bond length distributions across training settings. All panels show the MD reference alongside CG-BG proposals before and after reweighting. Results correspond to: (a) Flow trained on *unbiased* data (Core Beta); (b) Flow trained on *WT-MetaD* data (Core Beta); (c) Flow trained on *unbiased* data (Heavy Atom); (d) Flow trained on *WT-MetaD* data (Heavy Atom).